Contrib Mineral Petrol
DOI 10.1007/s00410-013-0932-z

ORIGINAL PAPER

Evolution of the Taupo Volcanic Center, New Zealand: petrological and thermal constraints from the Omega dacite

Sarah E. Gelman · Chad D. Deering · Francisco J. Gutierrez · Olivier Bachmann

Received: 21 February 2013 / Accepted: 18 July 2013

Abstract The 20 ka ~0.1 km^3 Omega dacite, which erupted shortly after the 26.5 ka Oruanui super-eruption, compositionally stands out among Taupo Volcanic Zone (TVZ) magmas, which are overwhelmingly characterized by rhyolites (>90 % by volume). The previously reported presence of inherited zircons in this zircon-undersaturated magma has provided unequivocal evidence for the involvement of upper-crustal material in a 1–10 year timescale prior to the Omega eruption. However, whether this crustal involvement is characterized by wholesale, melting of preexisting crust or subordinate bulk assimilation into an already differentiated magma body remains unclear. To disentangle these processes, we describe the mineral chemistry of the major phases present in the Omega dacite and determine intensive parameters describing magma chamber conditions. Dominantly unimodal populations of plagioclase ($An_{50–60}$), orthopyroxene (Mg# from 58 to 68), and clinopyroxene (Mg# from 65 to 73), along with coexisting equilibrium pairs of Fe–Ti oxides, constrain pre-eruptive temperatures to 850–950 °C, a pressure between ~3 and 7 kbars, and an oxygen fugacity of ~NNO. MELTS thermodynamic modeling suggests that this phase assemblage is in equilibrium with the bulk rock and glass compositions of the Omega dacite at these estimated P–T–fO_2 pre-eruptive conditions. Combining these petrological observations with insights into conductive thermal models of magma–crust interactions, we argue that the Omega dacite more likely formed in the mid-to-lower crust via protracted processing through fractional crystallization coupled with some assimilation (AFC). Incorporation of crustal material is likely to have occurred at various stages, with the inherited zircons (and potentially parts of glomerocrysts) representing late and subordinate upper-crustal assimilants. This petrogenetic model is consistent with the presence of a differentiating crustal column, consisting of a polybaric fractional crystallization and assimilation history. On the basis of petrological, thermal, and geophysical considerations, upper-crustal reservoirs, which feed large-scale rhyolitic volcanism in the TVZ, most likely take the form of large, long-lived crystal mush zones. Following large eruptions, such as the Oruanui event, this mush is expected to crystallize significantly (up to 70–80 vol% crystals) due to syn-eruptive decompression. Hence, the Omega dacite, immediately post-dating the Oruanui event, potentially represents incoming deeper recharge of less-evolved magma that was able to penetrate the nearly solidified upper-crustal mush. Over the past 20,000 years, similar intermediate recharge magmas have incrementally reheated, reconstructed, and reactivated the upper-crustal mush zone, allowing a gradual return to rhyolitic volcanism at the Taupo Volcanic Center.

Communicated by T. L. Grove.

Electronic supplementary material The online version of this article (doi:10.1007/s00410-013-0932-z) contains supplementary material, which is available to authorized users.

S. E. Gelman (✉)
Department of Earth and Space Sciences, University of Washington, Box 351310, Seattle, WA 98195-1310, USA
e-mail: sgelman@uw.edu

C. D. Deering
Department of Geology, University of Wisconsin–Oshkosh, 800 Algoma Blvd., Oshkosh, WI 54901-8649, USA

F. J. Gutierrez
Advanced Mining Technology Center, Universidad de Chile, 8370451 Santiago, Chile

O. Bachmann
Institute of Geochemistry and Petrology, ETH Zurich, Zurich, Switzerland

Published online: 04 August 2013

Keywords Silicic volcanism · Thermal modeling · Geochemistry · Petrology · Taupo Volcanic Zone

Introduction

Silicic magmas are thought to form through the combination of two end-member processes: crystal fractionation from mantle-derived mafic progenitors and partial melting of preexisting crust. The degree to which each of these processes has dominated throughout the Earth's history has major implications for the physical processes involved in, and the rate of, continental crust formation. On a more local scale, understanding the sources of silicic magmas in a given magmatic province can provide insight into the thermal, petrological, and tectonic structure of a region. Despite more than a century of research attempting to disentangle the relative contributions of mantle versus preexisting crust in the petrogenesis of evolved magmas (e.g., Bunsen 1851; Daly 1914; Bowen 1928), the complex geochemical signatures and frequent mixing of those two sources still fuel vigorous debate. For example, through a wide variety of experimental, observational, and theoretical techniques, some studies suggest a limited addition of preexisting crust to a more mafic, crystallizing progenitor that eventually evolves to produce silicic magma (e.g., Halliday et al. 1991; Thompson and Connolly 1995; Geist et al. 1998; Sisson et al. 2005; Simon et al. 2007; Jagoutz et al. 2009), while others suggest a dominant contribution from recycled crust (e.g., Conrad et al. 1988; Huppert and Sparks 1988; Petford et al. 2000; Riley et al. 2001; Price et al. 2005). A striking example of this controversy comes from oceanic arc lavas, where, in the same year, two different studies reported opposite interpretations for similar rocks in the same tectonic region (Haase et al. 2006; Smith et al. 2006).

With the advent of high-precision mass spectrometry and the broad use of isotopic tracers, the geochemical tools available to improve our understanding of magmatic processes occurring within the crust have grown considerably in the past few decades. Notably, it has been shown that open-system behavior (that is, contributions of mass from both mafic progenitor magmas as well as from country rocks) is the rule rather than the exception in magmatic systems, regardless of tectonic setting (e.g., Francis et al. 1980; Taylor 1980; Halliday et al. 1991; Dungan and Davidson 2004; Charlier et al. 2007; Davidson et al. 2007; McCurry and Rodgers 2009). Likewise, an ever-expanding library of experimentally and theoretically derived phase equilibria (e.g., MELTS, Ghiorso and Sack 1995) and the library of studies upon which it is built have broadened our available petrological tools, while the advancement of computational fluid dynamics and numerical heat transfer has most recently elucidated the possible physics at work in magmatic systems and their plausible relationships to the data, we can collect at the Earth's surface (e.g., Bergantz 1989; Petford and Gallagher 2001; Babeyko et al. 2002; Spera and Bohrson 2004; Annen et al. 2006; Dufek and Bachmann 2010; Gutierrez and Parada 2010; Huber et al. 2010). The goal of this study is to integrate the use of a few of these tools into a more unified approach toward examining the source of silicic magmatism within a spatially and temporally well-constrained system.

The Taupo Volcanic Zone (TVZ) in the northern island of New Zealand is ideally suited for this integrated study due to its relatively well-constrained crustal structure and well-documented eruptive history (Wilson et al. 1995; Smith et al. 2005). In particular, the Taupo Volcanic Center, location of the 26.5 ka, 530 km^3 Oruanui eruption (Wilson et al. 2006), affords us a unique opportunity to study the mechanisms involved in formation of silicic magma following the Oruanui caldera collapse, as the upper-crustal silicic magmatism was re-established. Here, we focus on one of the first post-Oruanui eruptions, the 20 ka Omega dacite, which constitutes only 0.1 km^3 of magma. Although small in volume, the appearance of this composition of magma is important since dacite has been proposed as the intermediate progenitor to the voluminous erupted rhyolites (Deering et al. 2008; Deering et al. 2011a), although dacites themselves rarely reach the surface in the TVZ ($\ll$1 % by volume of eruptive products).

We present petrological observations and mineralogical data constraining the P–T–fO_2 and water content under which the Omega dacite likely formed. Using these constraints, we also introduce thermal models to explore the influence that crustal melting has on the final composition, volume, and melt fraction of the Omega magma reservoir. Finally, we integrate our petrological observations with the thermal constraints to unravel the source contributions in the formation of the Omega dacite and discuss the potential insight that has been gained for understanding the formation of larger-scale silicic magmatism in the TVZ in general.

Background

Taupo Volcanic Zone (TVZ), New Zealand

The TVZ is located in the northern island of New Zealand (Fig. 1) amidst a basement of the mixed Permian to Cretaceous Torlesse and Waipapa terranes, which are generally composed of graywackes and sandstones (Pickard et al. 2000; McCormack et al. 2009). The TVZ is embedded in a back-arc basin associated with oblique subduction of the Pacific plate to the east, with current rates of extension in the northern island at least 8 mm $year^{-1}$

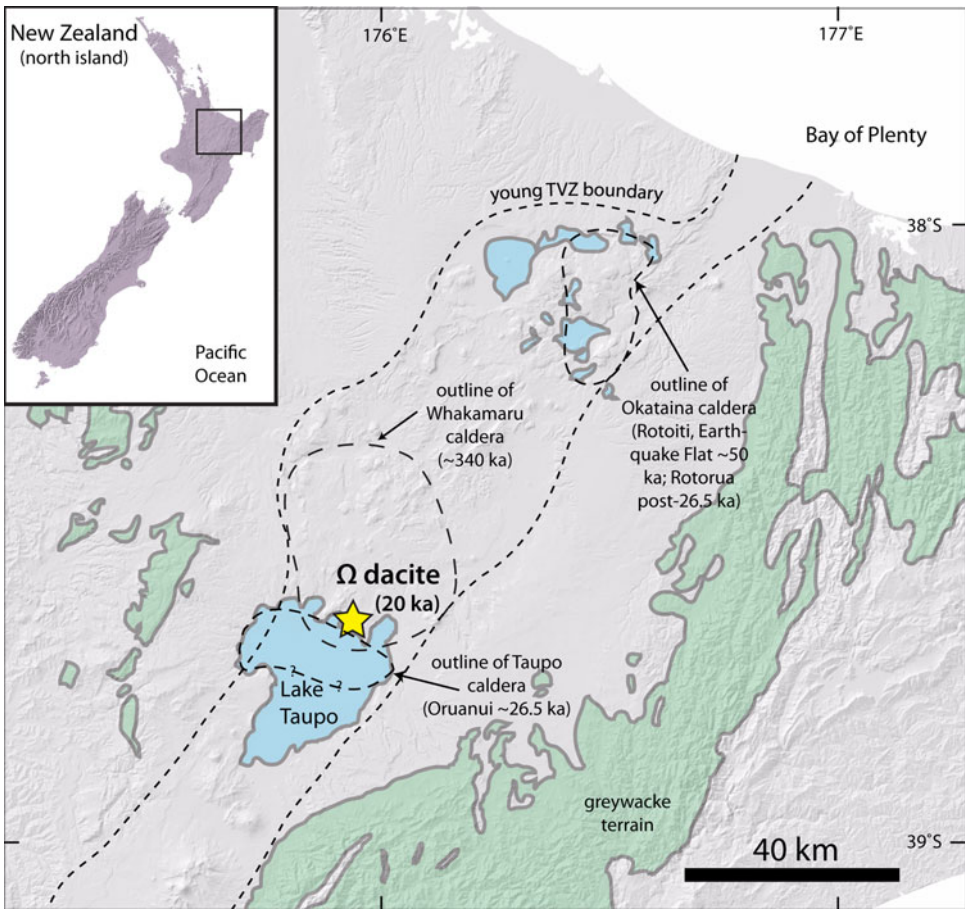

Fig. 1 Location map of the Taupo Volcanic Zone, New Zealand. A *star marks* the location of the primary outcrop of the Omega dacite, located near the northern shore of Lake Taupo. The young TVZ boundary is drawn after Wilson et al. (1995). The location of the Mesozoic metasedimentary terranes is drawn in *green* after New Zealand Geological Survey (1972)

(Darby et al. 2000). This has resulted in a thin, heavily intruded crust, with the upper 15 km composed roughly of quartzo-feldspathic lithologies, and a mafic, refractory lower-crustal region extending to 30 km depth (Harrison and White 2004, 2006; Stratford and Stern 2006).

The TVZ is one of the most voluminous and active rhyolitic magma systems on Earth (Wilson et al. 1995, and references therein). The TVZ has a total estimated volume of at least 10,000 km^3 erupted since 1.6 Ma, the great majority (≥90 %) of which is rhyolitic; the remainder is largely andesite, with rare basalts and dacites (Graham et al. 1995). Throughout the TVZ, the origin of silicic magmas has been a controversial topic for several decades (e.g., Ewart and Stipp 1968; Reid 1983; Graham et al. 1995; Price et al. 2005; Deering et al. 2008). In particular, Pb, Nd, Sr, and O isotopes by McCulloch et al. (1994) supported the contribution of up to 25 % assimilation of Torlesse graywackes, with the remaining contribution coming from extensive fractionation from a basaltic progenitor (AFC). Blattner et al. (1996) measured mineral oxygen isotopes and Sr isotopes, which were then interpreted as evidence for a subcrustal or lower-crustal origin for the TVZ magmas. However, the obvious compositional gap between basalts and rhyolites in the TVZ has been pointed out as evidence against fractionation from mafic end-members. Graham et al. (1992) and Graham et al. (1995) instead proposed the melting of andesitic forerunners and/or presumed lower-crustal granulites to reconcile both the isotopic data and the observed compositional gap. The recent model of Price et al. (2005) supports this idea, suggesting that andesite magmas that tend to freeze in the crust, but during the recent period of increased lithospheric extension, have been remelted to produce rhyolites. However, thermal modeling of magma emplacement, melt survival, and anatexis in lower-crustal arc environments has shown that melting of intermediate compositions is inefficient as a source of large volumes of silicic magmas (Dufek and Bergantz 2005; Annen et al. 2006). This motivated Deering et al. (2011a) to challenge the melting model of silicic magma petrogenesis in TVZ, and they instead proposed a model in which mantle-derived magmas with varying water contents and mineral crystallization sequences produce different evolving melts that correspond to either eruptible andesites or dacites that stall in the upper-crust resulting in silicic mushes. These mushes further process magmas through AFC to ultimately supply

rhyolites en masse to TVZ's more recent and voluminous eruptive centers.

The TVZ is composed of eight caldera centers, two of which are considered currently active: Taupo and Okataina Volcanic Centers (Smith et al. 2005). Within these systems, the youngest caldera-forming episode consisted of the Oruanui eruption at 26.5 ka, with an estimated magmatic volume of approximately 530 km^3 (Wilson et al. 2006). The Oruanui unit consists almost entirely of rhyolite, with the exception of rare mafic clasts (Sutton et al. 1995), and has been interpreted to have been assembled within ~40 kyr through a combination of crystal fractionation and secondary (≤10 %) melting and/or disaggregation of preexisting mush, plutons, and basement graywacke (Wilson et al. 2006; Charlier et al. 2008). However, despite all of these contributions, much debate still exists over the relative contributions of crystal fractionation from more juvenile magmas versus crustal assimilation to the overall Oruanui magma (see also Smith et al. 2005 for a brief, relevant summary of previous ideas).

Taupo Volcanic Center: 26.5 ka to present

Following the Oruanui eruption, there have been 28 documented eruptions in the Taupo Volcanic Center; the oldest three of these were dacitic and the remainder rhyolitic. Further details can be found in Wilson (1993), Sutton et al. (1995), and Smith et al. (2005), who have provided a more detailed summary of the events occurring in the Taupo Volcanic Center over the past 50 kyr, including the Oruanui and post-Oruanui magmas. Herein, we focus on the second eruption occurring in the Taupo Volcanic Center following the Oruanui eruption, the 20 ka Omega dacite (estimated volume of 0.1 km^3; Wilson 1993), on which Charlier et al. (2005) and Charlier et al. (2010) have performed detailed zircon geochronology.

Initial characterizations of the mineralogy and bulk composition of the post-Oruanui eruptive units carried out by Sutton et al. (1995) and Sutton et al. (2000) indicate that the Omega dacite should be significantly zircon-undersaturated. Indeed, no zircons were observed in thin sections during this study, which is expected given the noted rarity of zircons reported previously: Charlier et al. (2005) found 0.04 mg of zircon in 18 kg of crushed Omega pumice, giving a concentration of 0.0022 mg/kg (which is less than 1 % of the zircon-saturated Oruanui concentration of 0.9 mg/kg for comparison; their Table 2). However, when Charlier et al. (2010) did find zircons, a spectrum of ages from 0.2 to 1,149 Ma was observed. This provides unequivocal evidence for assimilation of preexisting wall rocks. While finding zircon xenocrysts is common in other large and small igneous systems around the world (e.g., Bindeman and Valley 2001; Lanphere and Baadsgaard 2001; Davidson et al. 2007; Bachmann et al. 2010), the observation is especially noteworthy in the under-saturated Omega dacite since these zircons should be susceptible to rapid dissolution. Yet, the zircons analyzed by Charlier et al. (2010) are euhedral and surrounded by glass; hence, they have interpreted this magma to be generated by wholesale melting of the crust and give a timescale for both the generation and eruption of the Omega dacite of 1–10 years. Understanding the origin of these xenocrystic zircons and, in particular, their relationship with the origin of the remaining Omega magma is critical to advance our understanding of how felsic magma is generated not only for the Omega dacite itself, but also for the entire TVZ and felsic magmatism in arc settings worldwide (Charlier et al. 2010).

Analytical methods

Mineral chemical data were collected on a JEOL 733 electron microprobe at the University of Washington equipped with an energy dispersive spectrometer and four wavelength dispersive spectrometers. For all minerals, an accelerating voltage of 15 kV was used. Beam size and current were varied according to the phase being analyzed: plagioclase and glass were analyzed with a 5 μm beam and 10 nA current; pyroxenes with a <1 μm beam and 15 nA current; Fe–Ti oxides with a <1 μm beam and 20–30 nA current. ZAF corrections were applied in all analyses. Calibrations were rechecked periodically on standards (including additional standards not used for calibrating), and Na was analyzed first for glass, plagioclase, and pyroxenes. Mineral analyses were considered acceptable when oxide totals were between 99 and 101 %, and formula unit cation totals were within a few percent of expected values. Counts, particularly during Na-measurements, were monitored during calibration to ensure negligible cation migration. For Fe–Ti oxides, *V* was measured on a different diffracting crystal (LIF) from Ti (PET) to ensure no primary peak overlap.

Petrological observations

The Omega dacite is a moderately crystal-rich (~25 % crystals) dacite, with a mineral assemblage that consists of plagioclase > orthopyroxene > clinopyroxene > titanomagnetite > ilmenite (Sutton et al. 2000). Apatite inclusions are ubiquitous in plagioclase, orthopyroxene, and clinopyroxene, and occur more infrequently included in Fe–Ti oxides. Pyrrhotite inclusions have been observed in plagioclase, ortho- and clinopyroxene, and Fe–Ti oxides. Plagioclase and pyroxenes are typically ~1–2 mm in diameter (although less frequently up to several mm) and

commonly occur as (often broken) euhedral to subhedral single crystals or as glomerocrysts of chemically similar crystals (Fig. 2). Detailed petrographic mapping of a thin section was aimed at producing a general textural description of the Omega dacite's crystal cargo. Of all the mapped crystallinity, the 2D area was composed of ~68 % plagioclase, 25 % pyroxenes, and 7 % oxides, in agreement with the calculations of Sutton et al. (2000). Glomerocrysts were counted when distinct crystals were unambiguously in contact, with the remaining crystallinity presumed to be phenocrysts. This analysis indicated that ~60 % of the crystallinity area consisted of glomerocrystic material, and the remaining ~40 % contained individual phenocrysts.

Mineral chemistry

Plagioclase

Plagioclase compositions vary from An_{45} to An_{85}, although the majority of clusters between An_{50} and An_{60} (Fig. 3a; Table 1). Complex oscillatory, but typically normal, zoning patterns are common, especially in single crystals (Fig. 4a, b). Rare, and small (<400 μm diameter), high An plagioclase amorphous zones can be found within both glomerocrysts (Fig. 5b) and single crystals (Fig. 5e). Occasionally resorbed, embayed, and inclusion-rich cores are observed (sieved textures), with later normally zoned regrowth; however, unlike the plagioclase crystals reported in Oruanui deposits (Charlier et al. 2008), no cloudy zones containing rutile needles were observed.

Pyroxene

Orthopyroxene and clinopyroxene compositions define a unimodal trend (i.e., single compositional population) with respect to Mg# [Fe recalculated based on stoichiometry, in mol% $Mg/(Mg + Fe^{2+})$]. Clinopyroxenes cluster fairly tightly between 65 and 73, while orthopyroxenes show more variability, ranging from 45 to 73, although most analyses cluster between 58 and 68 (Fig. 3b, c; Table 2). Both orthopyroxene and clinopyroxene sometimes display weak to moderate normal zoning in Mg#, with Mg-rich cores to Fe-rich rims (Fig. 4c). When present in

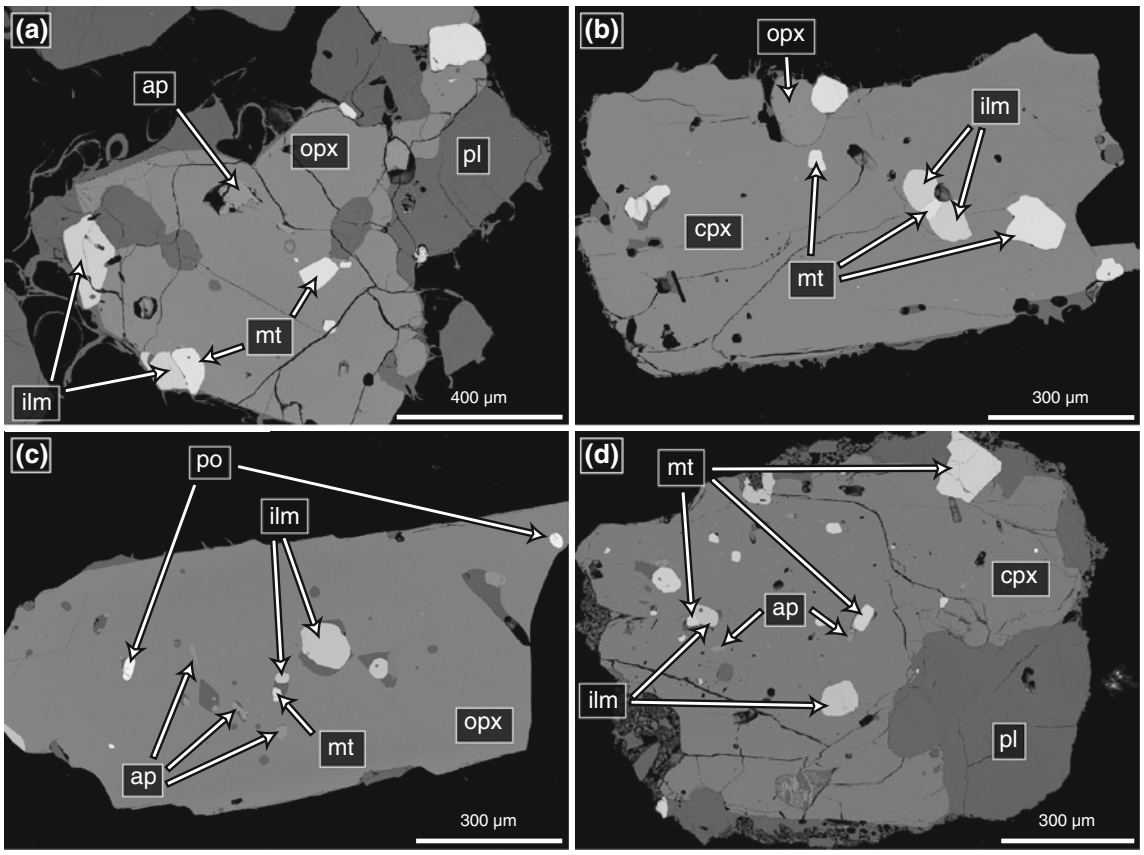

Fig. 2 Back-scattered electron (BSE) images of typical phenocryst morphology, textures, and inclusions. **a** Orthopyroxene–plagioclase glomerocryst with apatite, and coexisting ilmenite–magnetite inclusions. **b** Coexisting clinopyroxene–orthopyroxene with coexisting ilmenite–magnetite inclusions. **c** Orthopyroxene with magnetite, ilmenite, and pyrrhotite inclusions. **d** Glomerocryst of clinopyroxene and plagioclase with coexisting ilmenite–magnetite pair and apatites. *opx* orthopyroxene, *cpx* clinopyroxene, *pl* plagioclase, *mt* magnetite, *ilm* ilmenite, *ap* apatite, *po* pyrrhotite

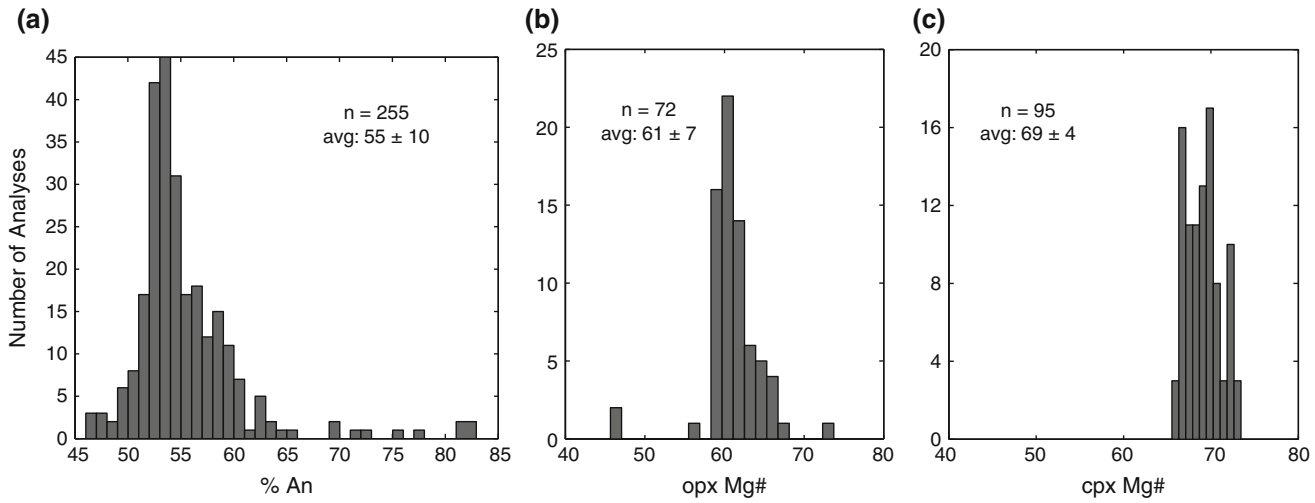

Fig. 3 Histograms of microprobe analyses of **a** plagioclase, **b** orthopyroxene, and **c** clinopyroxene. %An denotes the anorthite content of plagioclase. Mg# denotes the molar Mg/(Mg + Fe^{2+}) ratio in pyroxenes. *n* is number of analyses; average and 2σ error given for each panel

Table 1 Average glass and plagioclase analyses

n:	Average glass 46	Average plagioclase 56	High An plagioclase 1
SiO_2	73.81 (1.15)	54.33 (1.32)	45.97
TiO_2	0.46 (0.1)		0.46
Al_2O_3	13.89 (0.69)	28.32 (0.73)	33.23
FeO	3.04 (0.53)	0.51 (0.10)	0.52
MnO	0.09 (0.04)		0.07
MgO	0.44 (0.12)		0.41
CaO	2.23 (0.25)	11.36 (0.85)	16.64
Na_2O	3.22 (0.66)	4.98 (0.46)	2.01
K_2O	2.75 (0.19)	0.15 (0.05)	0
P_2O_5	0.07 (0.05)		0.06
Total		99.95 (0.37)	99.38
An		55.26 (4.15)	82.05

Average electron microprobe analyses of glass and plagioclase. Analyses performed at the University of Washington (S. Gelman analyst); 15 keV accelerating voltage, 5 μm beam, 10 nA current. *n* denotes number of points incorporated into average. Glass average composed of renormalized anhydrous analyses whose original oxide total was above 95 %. 2σ errors are given in parenthesis. Average plagioclase is composed only of analyses whose An content was calculated to be less than 67; all others are highly variable and rare, so a single example analysis is given in the third column (corresponds to the analysis of point shown in Fig. 5b)

glomerocrysts, pyroxenes often occur in contact with one another and in apparent textural equilibrium (Fig. 5a, b).

Fe–Ti Oxides

Ilmenite and titanomagnetite are ubiquitous throughout the Omega dacite, often in contact with one another (Fig. 2; Table 3). Fe–Ti oxides are generally rounded grains included in other phenocrysts, although they also can occur alone as individual phenocrysts. They frequently have pyrrhotite and apatite inclusions. No exsolution lamellae were evident in either phase. Neighboring pairs were the particular focus of microprobe work, but individual crystals were also analyzed. All adjacent pairs in contact were found to satisfy the Mn–Mg equilibrium criteria of Bacon and Hirschmann (1988). Indeed, nearly all permutations of ilmenites and titanomagnetites that were analyzed, whether as part of a pair or as individual crystals, satisfy the equilibrium criteria and hence could be used to determine intensive parameters (next section).

Glass

Although melt inclusions are present in almost all phases, we focused on analyzing glass adjacent to rims of orthopyroxene and clinopyroxene for estimation of pressure and temperature during the final stages of crystallization. However, additional analyses were performed on other regions of particularly fresh and well-polished glass, and within select melt inclusions adjacent to clustered minor phases (Fe–Ti oxides, pyrrhotite, and apatite). Only analyses with totals above 95 % have been used (although most totals were >97 %), and values reported here have been renormalized to 100 % anhydrous. In general, glass compositions indicate a low-to-moderate silica rhyolite (72–75 wt% SiO_2) and hence are slightly more silica rich than the composition reported by Sutton et al. (2000) of 70.5 wt% (Table 1). For all major oxides, these data suggest a single interstitial glass type with little variability.

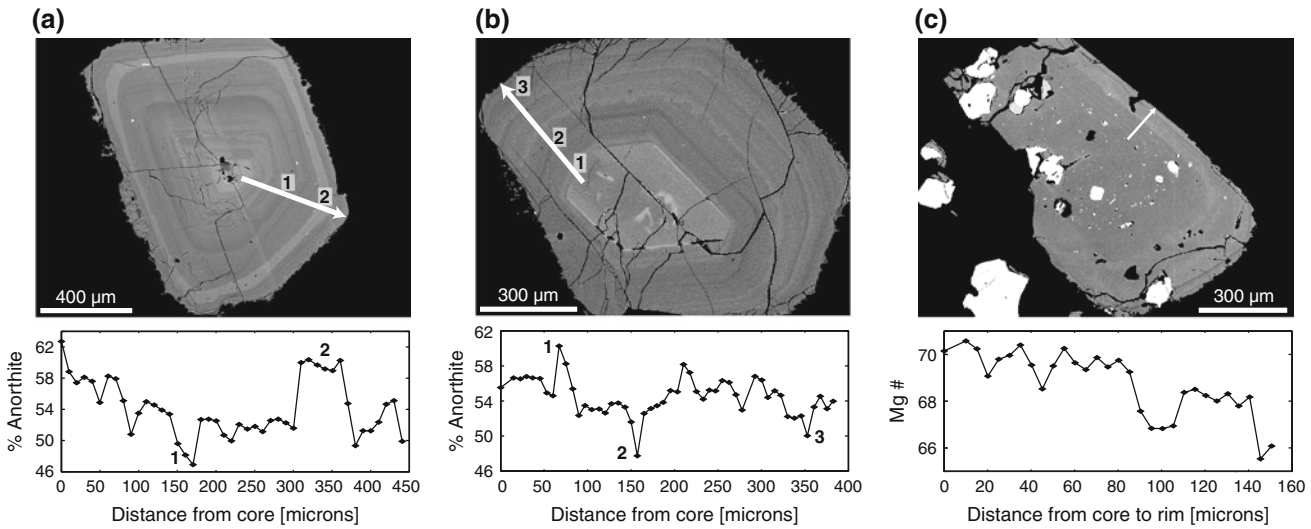

Fig. 4 Microprobe line scans of representative zoned crystals with back-scattered electron (BSE) images. **a** Plagioclase with a more anorthitic core and more albitic rim, and a prominent calcic spike at location 2. **b** Plagioclase with a dissimilar zoning morphology from **a**, but with nearly equal overall range in anorthite content. **c** Clinopyroxene profile in Mg# (molar Mg/(Mg + Fe^{2+})), with a magnesian core and iron-rich rim. We note in particular the general pattern of normal zoning in crystals in the Omega dacite, suggesting a down-temperature crystallization path

P–T–fO_2 conditions

Adjacent co-existing ilmenite–titanomagnetite pairs yield a consistent and limited range of temperatures and oxygen fugacities, constrained to approximately 912 °C ($\pm 2\sigma = 28°$) and NNO to NNO + 0.4 (where NNO denotes the nickel–nickel oxide buffer; Fig. 6), calculated using the geothermometer/oxybarometer of Ghiorso and Evans (2008). We note that these temperatures represent the latest conditions in the Omega magma reservoir prior to eruption, due to the fast kinetic re-equilibration of cations in Fe–Ti oxides (Pichavant et al. 2007).

The coexistence of clinopyroxene and orthopyroxene allows an independent estimation of temperature and pressure. For orthopyroxene and adjacent glass, using equation 28b in Putirka (2008), we find an average temperature of 871 °C ($\pm 2\sigma = 18°$). This is in excellent agreement with clinopyroxene and adjacent glass, which gives an average temperature of 882 °C ($\pm 2\sigma = 18°$) using equation 33 in Putirka (2008). It should be noted, however, that while these temperatures are all calculated from acceptable analyses that record consistently clustered compositions, adjacent glass and pyroxenes did not satisfy the equilibrium criteria of Fe–Mg partitioning given by Putirka (2008). This may reflect the fact that these calibrations do not adequately capture the partitioning of Fe^{3+} relative to Fe^{2+} in pyroxenes (Putirka, personal communication). We have also calculated temperatures based upon adjacent clinopyroxene and orthopyroxene pairs, which are in apparent textural equilibrium and lack any evidence for reaction rims. Using equation 36 in Putirka (2008), we find an average temperature of 893 °C ($\pm 2\sigma = 33°$). For all thermobarometers, input pressures were left blank in the absence of other definitive constraints, which resulted in better agreement between the three methods than an arbitrary initial guess of 3 kbars. For nearly all pairs, instead of an equilibrium Fe–Mg partition coefficient of ~1.09, these data consistently give ~0.7 (implying that the clinopyroxene FeO/MgO cation ratio is lower than that of the orthopyroxene). While these temperatures are generally higher than individual pyroxene–glass temperatures, they are consistent with calculated Fe–Ti oxide temperatures. One explanation for the difference in Fe–Mg partitioning between orthopyroxene and clinopyroxene is different crystallization depths, and, therefore, times. This, however, is not supported petrographically, since both pyroxenes have been observed to appear as inclusions in the other, and otherwise often appear intergrown. It is, however, possible that orthopyroxene crystallized over a greater time and temperature interval, which could explain enough discrepancy between the Fe and Mg partitioning to alter the average apparent behavior; this would be supported by the calculated temperatures of each phase, shown graphically in Figs. 5c and 6.

Corresponding pressures, calculated iteratively using the two-pyroxene thermobarometer (equation 38 in Putirka 2008), give a crystallization depth of 5–7 kbars. While clinopyroxene–glass supported this result, it also gave a much wider range, from −2.1 to 7.4 kbars (equation 30 in Putirka 2008). Finally, the orthopyroxene–glass barometer (equations 29a–c in Putirka 2008) gives clearly erroneous pressures of 0–0.4 kbars. Due to the lack of equilibrium as

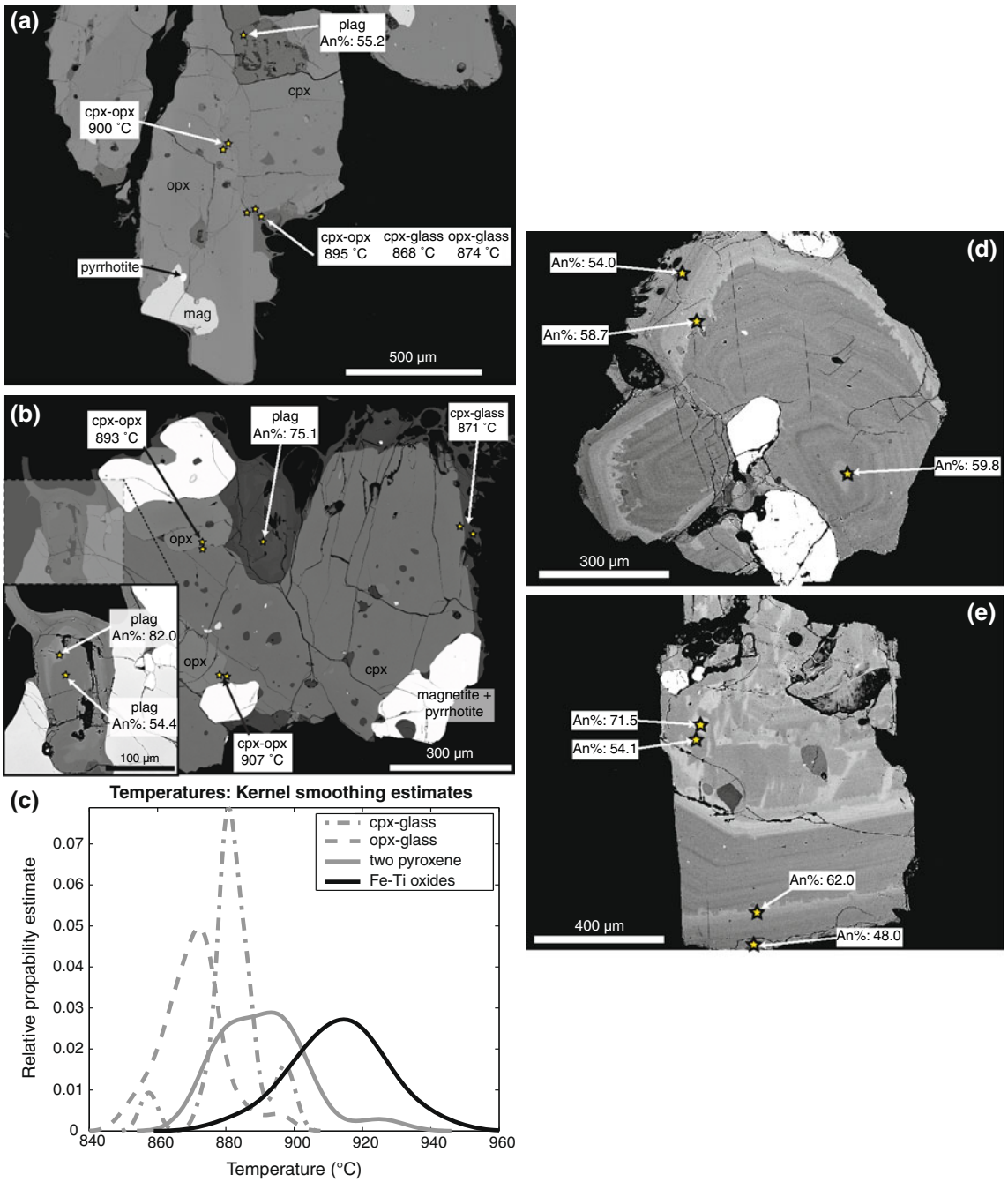

Fig. 5 **a**, **b** Samples of crystal aggregate textures, with some labeled plagioclase compositions and pyroxene calculated temperatures (back-scattered electron images). In **b**, note the portions of small plagioclase crystals that contain the very rare high anorthite compositions. In particular, in the *inset* plagioclase, only part of the crystal has a high anorthite content while the majority has a normal Omega composition (*grayscale* has been altered between the main part of **b** and the *inset* to highlight the high An region). **c** Kernel smoothing functions estimating the relative probability of temperatures resulting from the clinopyroxene–glass, orthopyroxene–glass, clinopyroxene–orthopyroxene, and Fe–Ti oxide thermometers (reported in '*P–T–f*O_2 conditions' section). **d** Glomerocrystic plagioclase with roughly normal zoning, and a prominent resorption feature about 100 µm into the crystals. **e** A single crystal of plagioclase with >400 µm of normal zoning, a similar resorption feature to the crystals in **d**, but with a sieve texture core, containing melt inclusions and high An zones

indicated by Fe–Mg partitioning, as well as the fact that these thermobarometers are truly only calibrated for clinopyroxene compositions of Mg# > 75 (which is higher than the range observed in the Omega dacite; Fig. 3), we stress that caution should be exercised before attempting to utilize these pressure estimates.

Table 2 Average pyroxene analyses

Mineral *n*:	Clinopyroxene 95	Orthopyroxene 72
SiO_2	52.12 (1.07)	52.30 (1.41)
TiO_2	0.41 (0.21)	0.24 (0.17)
Al_2O_3	1.65 (0.99)	0.91 (0.78)
Cr_2O_3	0.01 (0.02)	0.02 (0.03)
FeO^T	11.06 (1.44)	23.66 (4.04)
MnO	0.48 (0.09)	0.83 (0.22)
MgO	13.90 (0.90)	20.81 (2.76)
CaO	19.78 (0.91)	1.29 (0.44)
Na_2O	0.29 (0.06)	0.02 (0.02)
Total	99.72 (0.68)	100.09 (0.82)
Mg#:	69.15 (3.83)	61.04 (7.18)
%En	40.18 (2.13)	58.63 (6.73)
%Wo	41.11 (1.38)	2.60 (0.88)
Cpx–glass temperature P.Eq.33 ($n = 17$)	882 (18)	
Cpx–glass pressure P.Eq.30	5.4 (4.0)	
Opx–glass temperature P.Eq.28b ($n = 26$)	871 (18)	
Opx–glass pressure P.Eq.29a	−0.1 (0.2)	
Cpx–Opx temperature P.Eq.36 ($n = 21$)	893 (33)	
Cpx–Opx pressure P.Eq.39	6.5 (1.8)	

Average electron microprobe analyses of clinopyroxene and orthopyroxene. Analyses performed at the University of Washington (S. Gelman analyst); 15 keV accelerating voltage, 15 nA current. Total Fe reported as FeO^T, while totals are reported after recalculating the proportion of Fe^{2+} and Fe^{3+}. %En is calculated as 100 * Mg/(Mg + Fe^{2+} + Ca + Mn) and %Wo as 100 * Ca/(Mg + Fe^{2+} + Ca + Mn). 2σ errors reported in parenthesis. Results of pyroxene thermobarometers from Putirka (2008) are reported; units for temperature are °C and pressure are kbars. All thermobarometers were given blank input pressures. See text for 'Discussion' on this choice, as well as details and problems associated with the application of these thermobarometers to the Ω dacite

Table 3 Average co-existing Fe–Ti oxide analyses

Mineral *n*:	Magnetite 16	Ilmenite 18
SiO_2	0.00 (0.01)	0.00 (0.00)
TiO_2	13.24 (0.93)	45.85 (1.19)
Al_2O_3	2.36 (0.16)	0.23 (0.03)
Cr_2O_3	0.06 (0.04)	0.01 (0.02)
FeO*	76.72 (1.14)	48.07 (0.76)
MnO	0.48 (0.06)	0.58 (0.06)
MgO	1.69 (0.21)	2.69 (0.25)
ZnO	0.10 (0.05)	0.03 (0.04)
V_2O_3	0.60 (0.22)	0.32 (0.09)
Total[a]	99.31 (0.74)	99.16 (1.00)
G&E-08: *T* (°C)		912 (28)
G&E-08: ΔNNO		0.17 (0.20)

Electron microprobe analyses of adjacent or touching magnetite-ilmenite pairs. Analyses performed at the University of Washington (S. Gelman analyst); 15 keV accelerating voltage, 30 nA current. All pairs satisfy the equilibrium criteria of Bacon and Hirschmann (1988). Individual pair temperatures and oxygen fugacities calculated based on Ghiorso and Evans (2008), denoted G&E-08, shown in figure. FeO*, total iron as Fe^{2+}. *n*, number of analyses. [a]Total after recalculating the proportions of Fe^{3+} and Fe^{2+}. Numbers in parentheses are the 2σ

Other published results on two-pyroxene dacites generally suggest a crystallization depth equivalent to the mid-crust (~3+ kbars). For example, the Toba magma system erupted the 1.2 Ma two-pyroxene Haranggoal dacite (HDT), with pyroxene compositions remarkably similar to those of the Omega dacite (opx En% 58–61 and cpx En% 39–40, their Table 7; Chesner 1998). Although pressures were not estimated for that particular unit, all other Toba units (amphibole-bearing rhyolites) gave estimates of 2–3 kbars. In his model of the Toba system, Chesner (1998) places the HDT magma reservoir under these more evolved rhyolitic reservoirs, thus proposing 3 kbars as a reasonable minimum pressure estimate. Another similar dacitic unit in the TVZ, the Hauparu magma (albeit with slightly more albitic plagioclase compositions and more Mg-rich pyroxenes), yields pressure estimates from 2.8 to 5 kbars (Shane et al. 2005).

The dissolved water content in the melt of the Omega magma was calculated using the plagioclase hygrometer from Lange et al. (2009). While recognizing the uncertainty associated with the above pressure estimates, we test a range of pressures (3, 5, 7 kbars), an input temperature of 900 °C, and a plagioclase composition of An_{55}; we find a range from 4.3 to 4.7 wt% H_2O using the Omega bulk rock composition (Sutton et al. 2000) and 4.7–5.2 wt% H_2O using the Omega glass composition (Sutton et al. 2000). Considering that the Omega dacite does not appear to be very water rich (no amphibole or biotite, which are found in other felsic rocks in TVZ), these calculated H_2O concentrations appear to be maximum estimates. Indeed, experiments discussed in the next section by Eggler (1972), Geschwind and Rutherford (1992), and Costa et al. (2004) on intermediate bulk compositions at mid-to-upper crustal depths find that wt% H_2O must be less than ~4 in order to suppress the crystallization of amphibole.

Pre-eruptive petrological equilibrium

Here, we utilize the thermodynamic software package MELTS (Ghiorso and Sack 1995) as a tool to examine the stability fields of the mineral phases observed in this study,

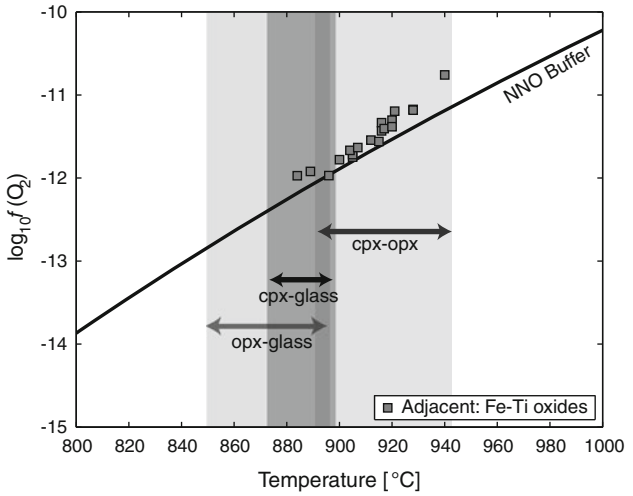

Fig. 6 Summary of temperature and oxygen fugacity calculations. *Shaded* are the fields for the temperatures calculated using adjacent clinopyroxenes, orthopyroxenes, and glass, using the calibrations of Putirka (2008). Plotted are the calculated temperatures and oxygen fugacity of adjacent Fe–Ti oxides based on the calibration of Ghiorso and Evans (2008)

for the range of reasonable intensive conditions determined in the previous subsection. A series of MELTS experiments beginning with the bulk rock composition (Sutton et al. 2000), conducted over a range of pressures (from 2 to 6 kb), with a range of bulk rock water contents (from 1 to 4 wt% H_2O), a constant fO_2 of NNO, and run from the liquidus down to 800 °C in equilibrium mode, broadly suggests that the *major* mineral phases present in the Omega dacite (plagioclase, and two pyroxenes) are in equilibrium with their surrounding melt (Fig. 7). The main observations are the following:

- Other than at high pressures (>4 kbars, in which garnet becomes stable) and extremely low water contents (≤1 wt% in which quartz becomes stable), no minerals other than those observed in the Omega dacite appear in MELTS simulations.
- Plagioclase is stable throughout the suite, although MELTS always predicts lower anorthite content (by about 10–15 mol% An) than that observed in the actual Omega data.
- Typically, ilmenite is stable at high pressures and low water contents, while the opposite is true for magnetite.
- While orthopyroxene is largely stable throughout the suite, clinopyroxene appears stable mainly at higher water contents, higher pressures, and lower temperatures.
- Residual melt compositions were compared with that observed in the Omega dacite, and broadly match at 1–3 wt% H_2O. While this water content is consistent with the observation of no hydrous phases, it is significantly lower than that predicted by the plagioclase-liquid hygrometer.

These MELTS results are corroborated by various experiments performed on other intermediate compositions

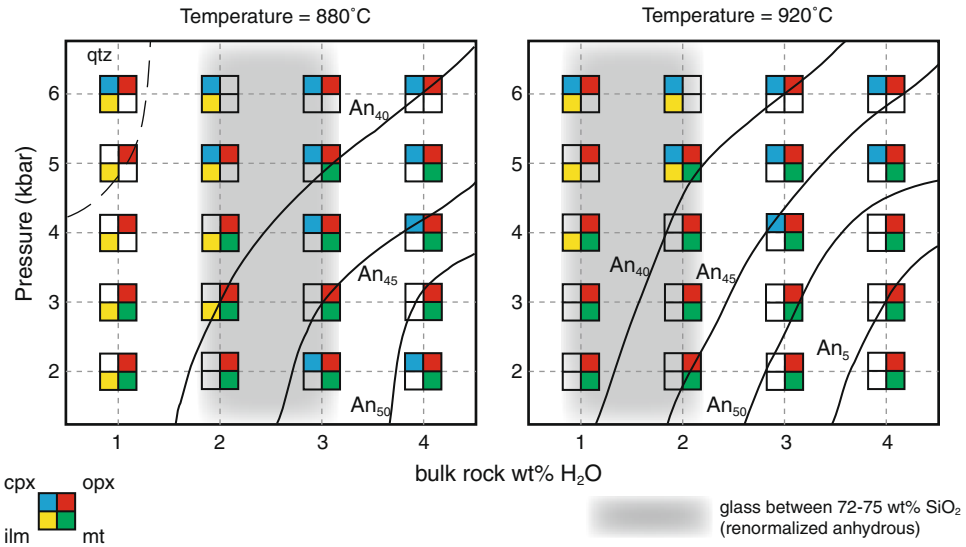

Fig. 7 Results of MELTS simulations exploring the stability of phases in the range of intensive parameters expected for the Omega dacite. *Left panel* represents runs at 880 °C, while *right* is at 920 °C. Pressure is plotted against bulk rock water content, and initial composition is the bulk rock given by Sutton et al. (2000). Plagioclase is always stable, and plotted curves outline the approximate stability fields for various predicted anorthite contents, noting that a range of An_{50-60} is normally observed in the Omega dacite. *Shaded* in the background is an anhydrous liquid SiO_2 content in agreement with observations of Omega glass. From these theoretical experiments, we conclude that the phase assemblage observed in the Omega magma (*plag*, *cpx*, *opx*, *mt*, *ilm*) is consistent with an equilibrium phase assemblage given the bulk rock composition and estimates on pressure, temperature, oxygen fugacity, and water content

at varying water contents and upper-to-mid crustal depths. In particular, the water content predicted by MELTS is consistent with a lack of amphibole in the Omega magma, which is supported by several previous studies such as by Eggler (1972) and Geschwind and Rutherford (1992). Moreover, compared with experimental runs under similar conditions (bulk initial composition, temperatures, pressures, oxygen fugacities, aH_2O), we find good agreement in terms of predicted stable mineralogy between the phase diagram presented by Costa et al. (2004) and the phenocrysts actually observed in the Omega dacite.

The observation of an equilibrium phase assemblage supports a 'down-temperature' hypothesis in which phenocrysts crystallize from a cooling magma. This observation is compatible with a petrogenetic model dominated by fractionation from mafic parents. However, it could also be argued that a pocket of crustal melt that pooled in an upper-crustal reservoir could also crystallize those equilibrium phases. Thus, in the following section, we develop thermal models to further explore the thermal limitations of these two end-member processes: (1) intrusion of a basaltic 'hot plate' producing the Omega magma via wholesale crustal melting and (2) intrusion of a dacite inducing bulk assimilation.

Thermal modeling

Zircons liberated through the melting and/or disaggregation of graywacke and granodiorite country rocks in the zircon-undersaturated Omega dacite suggest a 1–10 year timescale for the process of assimilation to occur (Charlier et al. 2010). Two end-member mechanisms have been proposed to describe this rapid zircon liberation process (Charlier et al. 2010): (1) partial crustal melting and extraction of that melt into the host magma and (2) wholesale melting and disaggregation of country rock as a single source for the magma. Within this theoretical framework, thermal models can be used to examine the range and types of conditions expected in each of these scenarios, explore a range of appropriate parameter spaces such as the depth and geometry of magma emplacement, determine the composition and initial temperature of the emplaced magma, and ultimately constrain the expected production of crustal melt during this timescale. We consider two end-member conceptual models for the formation of the Omega dacite and the assimilation of xenocrystic zircons to guide the setup of our thermal models, aimed at capturing the hypothetical mechanisms identified above: (1) intrusion of a basalt, contributing heat but not significant mass, to produce wholesale melting (importantly, mass cannot be contributed from the basalt, since the graywacke country rock bulk composition is already similar to the Omega dacite, and there is a lack of any observations suggesting mixing) and (2) intrusion of a dacite, capable of contributing both heat and mass toward a crustally contaminated magma. In both cases, successful models should produce ~ 0.1 km^3 of *mobile dacitic* magma, which we define conservatively as magma containing at least 50 % melt.

Conductive thermal models were constructed using COMSOL Multiphysics v3.5a and solve the heat equation using the finite element method:

$$\rho C_p \frac{\partial T}{\partial t} + \rho L \frac{\partial \chi}{\partial T}\frac{\partial T}{\partial t} = \nabla(k\nabla T)$$

where ρ is density, C_p is specific heat capacity, T is temperature, t is time, L is latent heat of crystallization, χ is melt fraction, and k is thermal conductivity. Models are two-dimensional axisymmetric and consider a range of geometries, from sill-like (radius is 1,000 m) to stock-like (radius is 250 m). In all cases, 0.1 km^3 of magma is emplaced instantly and allowed to cool and melt the crust. Melt survival in the intrusion is tracked, along with melt production in the crust. Since models are static, no assumption regarding melt extraction is made, and hence, the results are designed to overestimate real volumes of eruptible magma, which would be restricted normally to only high melt fraction regions (Marsh 1981). As a proxy for depth, ambient country rock temperatures are varied from 200 to 600 °C. Two main compositions are tested as the intruding magma: a primitive basaltic end-member (K-Trig, Table 1, Gamble et al. 1993) and generalized dacite/granodiorite mimicking the predicted crystallinity temperature path derived from MELTS modeling of the Omega dacite (Fig. 8).

Material properties are considered as a mixture of melt and solid components for each composition; for example, the density of country rock is defined as $\rho_{cr} = (\rho_{cr,L}\chi_{cr}) + (\rho_{cr,S}(1-\chi_{cr}))$, where the subscripts L and S correspond to the liquid and solid values, respectively. Since the Omega dacite is similar in bulk composition to the proposed anatectic composition of granodiorite and graywacke, the same dacitic composition is used for the country rock (values denoted *d*, for dacite, in Table 4). Specific heat capacity for basaltic and dacitic melts, and temperature-dependent values for the solids, defined using the bulk Omega dacite and K-Trig compositions, are given by Spera (2000). Using the precisely measured temperature-dependent thermal diffusivity of Whittington et al. (2009), a temperature-dependent thermal conductivity is derived. The remaining constant thermal properties are given in Table 4. Modeling geometry is shown schematically in Fig. 9a, and two example simulations are illustrated in Fig. 9b (sill-like intrusion of K-Trig basalt) and Fig. 9c (stock-like intrusion of dacite).

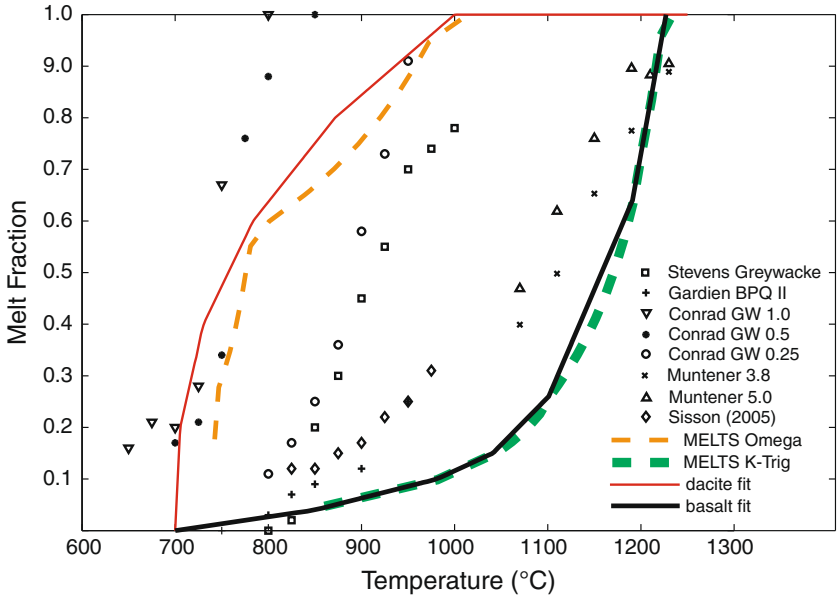

Fig. 8 Summary of melt fraction–temperature relationships observed in various experimental studies and those ultimately used in thermal models. Sources for experimental data: *squares* are graywacke from Stevens et al. (1997); *plus symbols* are graywacke from Gardien et al. (1995); *upside-down triangles*, *stars*, and *circles* are graywacke with varying water contents from Conrad et al. (1988); *cross-symbols* and *upward-facing triangles* are basalts with varying water contents from Muntener et al. (2001); and *diamonds* are basalt (87S35A) from Sisson et al. (2005). The *thin dashed* (*orange*) curve is a MELTS simulation using the Ω dacite bulk rock composition, NNO, 2 kbars, and 3 wt% H_2O; while the shape of this curve did not change significantly between using MELTS or rhyolite-MELTS (Gualda et al. 2012), neither thermodynamic model gave very stable results at melt fractions below ~0.6. The *thick dashed* (*green*) curve is the MELTS results for K-Trig (Gamble et al. 1993) at NNO, 5 kbars and 0.5 wt% H_2O. Note that, this *thick dashed* (*green*) curve is virtually identical to MELTS simulations at 3 and 4 kbars for the mafic end-member calculated for the Oruanui by Wilson et al. (2006) in their Table 7. Finally, two intrusion compositions were tested in thermal models: a graywacke/granodiorite/dacite fit to experimental data and MELTS simulations (*thin red/gray curve*) and basalt fitted to MELTS simulations (*thick black curve*)

Table 4 Thermal modeling parameters

Symbol	Parameter	Value
$\rho_{L,b}$	Density of basalt melt	2,680 kg/m^3
$\rho_{S,b}$	Density of basalt solid	2,940 kg/m^3
$\rho_{L,d}$	Density of dacite melt	2,370 kg/m^3
$\rho_{S,d}$	Density of dacite solid	2,500 kg/m^3
L_b	Latent heat of basalt solidification	396 kJ/kg
L_d	Latent heat of dacite solidification	354 kJ/kg
$C_{p,L,b}$	Specific heat of basalt melt	1,484 J/kg/°C
$C_{p,L,d}$	Specific heat of dacite melt	1,388 J/kg/°C

Modeling results

Since very little heat is transferred from the intrusion to the crust in only 1 year, most results are given at the upper end of the estimated timescale for zircon dissolution (10 years). Models were run out to 100 years to give a better understanding of the evolving melt formation and survival through time. Results are described in terms of both the total volume of melt (V_{melt}, not including any crystalline material) and the total volume of mobile magma (V_{mob}, including both melt and crystals, but melt fraction is required to be greater than 0.5). For convenience, we also define the following parameters: R_{melt} is the volume of crustal melt produced, divided by the volume of residual melt remaining in the intrusion ($V_{melt,cr}/V_{melt,in}$, does not include any crystalline material) and R_{mob}, which is the volume of mobile magma produced in the crust, divided by the volume of residual mobile magma remaining in the intrusion ($V_{mob,cr}/V_{mob,in}$, including both melt and crystals, but with melt fraction greater than 0.5). A summary of results is given in the Supplementary Table 1A, and selected results are shown in Figs. 9 and 10.

As expected, the cases predicting the most anatectic melt were intrusion of high temperature mafic magmas into crust with a high ambient temperature of 600 °C. In the cases of basaltic intrusion, a high initial intrusion temperature results in a steeper temperature gradient leading to quicker heat loss from the intrusion to the crust. This results in greater generation of crustal melt with quicker freezing of the initial intrusion, thereby producing higher R_{melt} and R_{mob} values than dacitic intrusions. In addition to the effect of a higher initial intrusion temperature, basaltic magma tends to crystallize more at higher temperatures, which is opposite of more silicic magmas (Fig. 8). The nature of the melt fraction–temperature relationship of

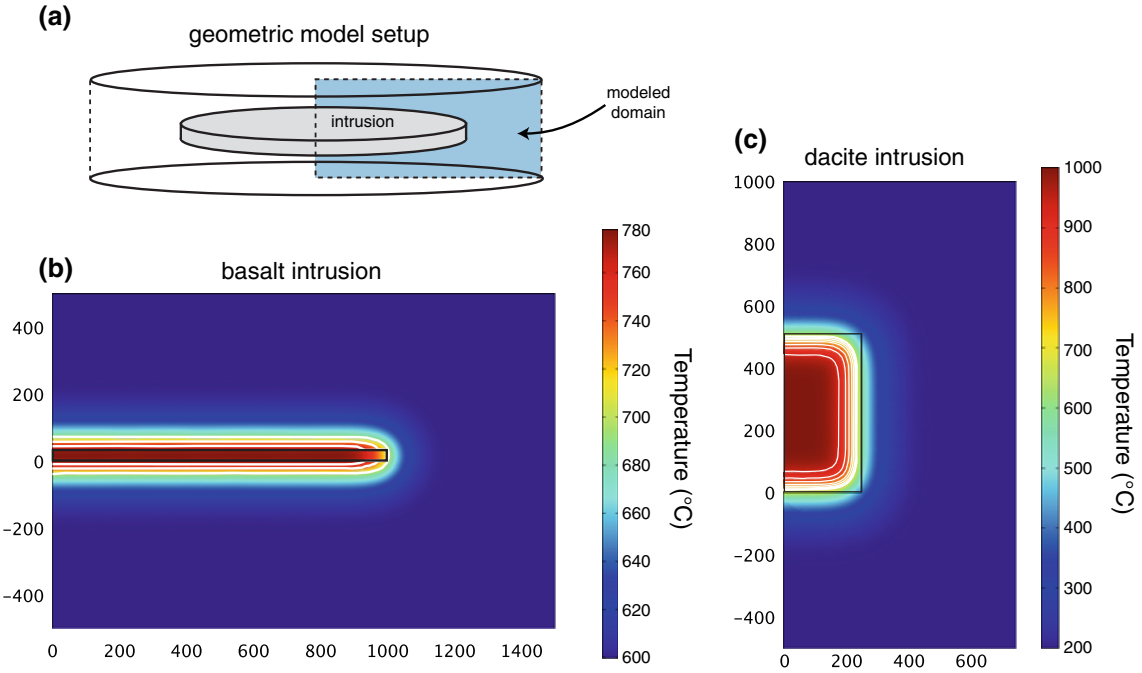

Fig. 9 Thermal modeling geometry with example simulations. **a** Schematic representation of the 2D axisymmetric geometry; note the cylindrical crustal column and sill in the center. A flat 2D panel is the actual modeled domain, with volumes and fluxes integrated through the third dimension. **b** Example simulation of a sill-like geometry (radius = 1,000 m) using the basaltic intrusion composition and an ambient crustal temperature of 600 °C. **c** Example simulation of a stock-like geometry (radius = 250 m) using the dacitic intrusion and ambient crustal temperature of 200 °C. In both **b** and **c**, the *colorbar* shows temperatures, and *white contours* show melt fractions

silicic country rock then results in its tendency to rapidly increase melt fraction in response to small temperature increases above the solidus, while the basalt rapidly decreases melt fraction as it cools from its liquidus. Hence, basaltic intrusions should preserve greater amounts of crustal melt, and less of the residual intruded melt, when compared with dacitic intrusions (which have approximately the same bulk composition as the country rock). Thus, in agreement with previous numerical studies of basalt–crust interactions with variable phase diagrams (e.g., Dufek and Bergantz 2005; Annen et al. 2006), these models illustrate the tendency of hot, mafic intrusions to favor production of crustal melt at the expense of intrusion survival.

Ambient country rock temperature plays an important role in determining both the amount of crustal melt produced, as well as the amount of intrusive melt surviving. This is quantitatively illustrated in Fig. 10, which shows the results of basaltic sill-like intrusions (set up shown in Fig. 9b) and dacitic stock-like intrusions (set up shown in Fig. 9c). In the cases of basaltic sill-like intrusions, most of the intrusive melt freezes, and hence, the most obvious effect of variations in ambient temperature is on evolution of the surrounding crust (i.e., determining how much of the original intrusion's heat is divided into sensible heat, raising the country rock temperature to its solidus, versus latent heat, causing partial melting). On the other hand, dacitic stock-like intrusions retain most of their intrusive melt, producing little or no crustal melt; hence, ambient crustal temperatures have a more minor influence on magma production and survival overall. Again, due to the temperature gradient setup between the country rock and the intrusion, heat loss is quicker with lower ambient temperatures, and thus, less of the intrusion is expected to survive, regardless of how much (or little) country rock is melted.

As shown in Fig. 10b, basaltic sill-like intrusions can lose virtually all of their residual intrusive mobile magma ($V_{\mathrm{mob,in}}$) in just 10 years, in contrast with dacitic intrusions of any geometry and basaltic stock-like intrusions. The rapid and complete crystallization of the intrusive material leads to very high R_{mob} values. However, in all other scenarios (in which residual intrusive mobile magma does remain), R_{mob} never exceeds $\sim$0.3 in 10 years (Fig. 11). This illustrates the general inefficiency of mid-to-upper crustal wholesale melting, even for the basaltic underplating case (except for highly elevated geothermal gradients). Thus, we infer that stock-like basaltic and (independent of geometry) dacitic intrusions favor limited, subordinate assimilation, rather than prolific crustal anatexis, as a model for silicic magma production, since crustal mobile magma volumes are always significantly lower than residual intrusion mobile magma volumes. Similar conclusions were reached through modeling by Dufek and Bergantz (2005) and Annen et al. (2006).

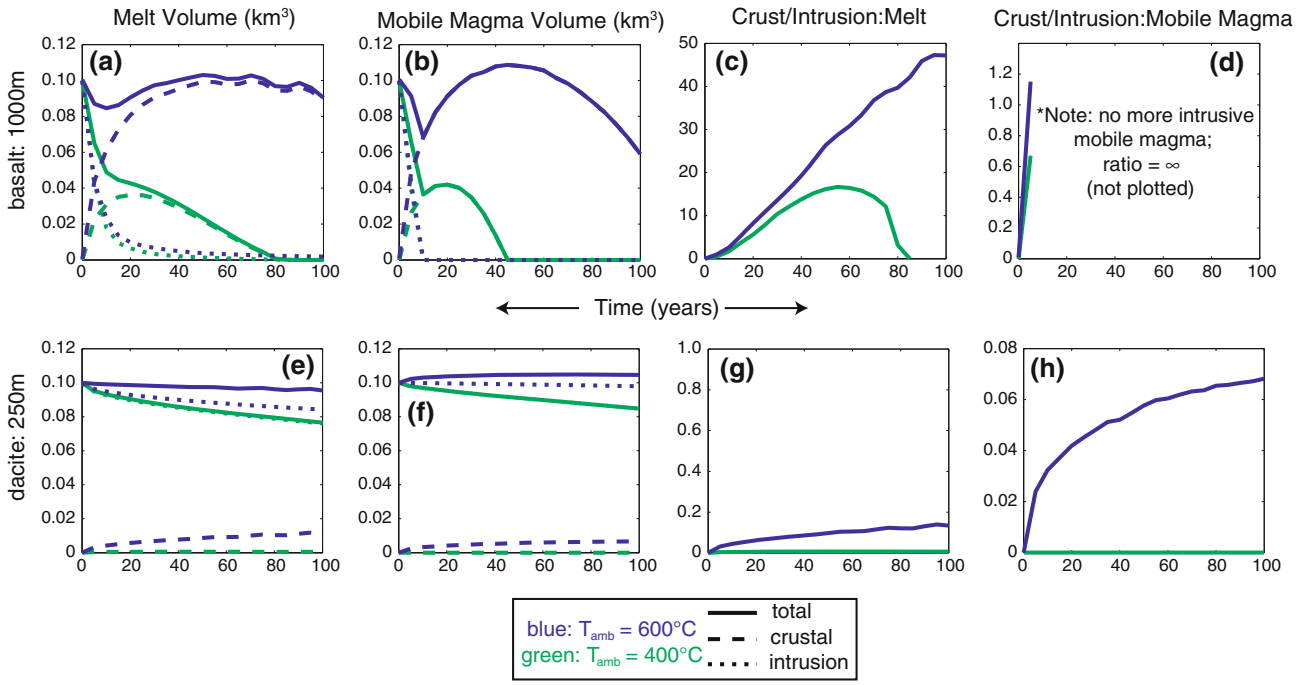

Fig. 10 Example modeling results: the *first row* corresponds to the model setup illustrated in Fig. 9b; the *second row* corresponds to the model setup illustrated in Fig. 9c. **a**, **e** Total melt volume through time (V_{melt}); **b**, **f** Total mobile magma volume through time (V_{mob}); **c**, **g** Volume of generated crustal melt divided by the volume of residual intrusive melt (R_{melt}); **d**, **h** Volume of generated crustal mobile magma divided by the volume of residual intrusive mobile magma (R_{mob}). Note in **d** that no mobile magma existed after a few years for the sill-like basaltic intrusions, and hence, R_{mob} was undefined (and not plotted). In **a**, **b**, **e**, and **f,** *solid lines* are total melt/mobile magma, *dashed lines* are crustal melt/mobile magma, and *dotted lines* are intrusion melt/mobile magma. *Black* and *gray* correspond to ambient temperatures of 600 and 400 °C, respectively

Second order results of the thermal models further define the effect of intrusion aspect ratio on the tradeoff between crustal melt production and the survival of high temperature, high melt fraction magma. The emplacement of a sill-like geometry maximizes the surface area through which heat can be transferred to the crust. While this causes more widespread crustal melting (generally increasing R_{mob} and R_{melt}), it also causes a more diffuse zone of melt, both in the intrusion and surrounding it, which results in *very low-melt fraction* magma (thereby decreasing V_{mob}). Thus, an additional modeling result is that sill-like intrusions are poor generators of large volumes of eruptible magmas. Contrarily, stock-like intrusions have a lower surface area in contact with surrounding crust, and, therefore, cause less anatexis while sustaining an insulated, hot core of mobile magma. These results are illustrated in Fig. 11, in which stock-like intrusions are predicted to have larger volumes of mobile magma, consistent with the more complex simulations of Gutierrez and Parada (2010), which included both convection and a more realistic treatment of crystal–fluid–melt interactions.

Discussion: determining the relative contributions of crustal versus mantle sources for the Omega dacite

Building on the mineralogical data and intensive parameters reported in 'Petrological observations' section, and integrating the results of the thermal models in the above section, here, we discuss possible models for the formation of the Omega dacite. Starting with an end-member model of rapid wholesale crustal melting, we compare expectations for mineralogical textures and chemistry with an alternative model proposing late, limited bulk assimilation by a dacitic magma produced predominantly by assimilation–fractional crystallization (AFC).

The 'up temperature' melting model

While recognizing that great heterogeneity exists in the basement metasediments in New Zealand, here we utilize published experimental data to assess the possibility of melting of graywacke and granodiorite to produce a magma that is compositionally and mineralogically similar to the Omega dacite. Conrad et al. (1988) conducted

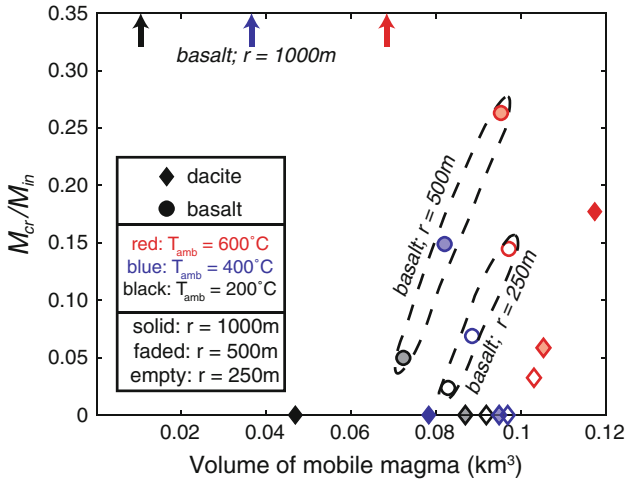

Fig. 11 Thermal modeling results after 10 simulated years of evolution: volume of total mobile magma (V_{mob}) as a function of the volume of crustal mobile magma divided by intrusive mobile magma (R_{mob}). Models with a basaltic intrusion are *circles*; dacite intrusions are *diamonds*. *Symbol line* color corresponds to ambient country rock temperature. *Solid symbols* indicate a sill-like geometry ($r = 1{,}000$ m), *faded interior* of *symbols* indicates intermediate aspect ratios ($r = 500$ m), and *empty symbols* indicate stock-like geometry ($r = 250$ m). To facilitate discussion, the basalt models have been outlined according to geometry to illustrate the trade-off between increasing proportion of crustally derived mobile magma, at the expense of total volume of mobile magma. Similarly, all dacite intrusions with ambient country rock temperatures below ~600 °C produce insignificant quantities of crustal mobile magma

experiments specifically aimed toward melting both relevant dacitic and graywacke compositions to test the production of TVZ rhyolites. However, these experiments were conducted at 10 kbars, which invariably led to the stability of garnet as a peritectic phase during melting. Two commonly used trace element ratios indicating the involvement of garnet in a magmatic source are high Sr/Y (e.g., Martin 1999) and high chondrite-normalized La/Yb (e.g., Drummond and Defant 1990). As shown in the Supplementary Material, the Omega dacite bulk pumice and glass (data from Sutton et al. 2000) give very moderate or low values of Sr/Y (9.3 to 9.7 for single pumices and 6.4 for glass) and $(La/Yb)_N$ (4.76 for single pumice and 4.67 for glass). Thus, since there is no evidence for the involvement of garnet in generating the Omega magma, we are unable to utilize the results of Conrad et al. (1988) to examine the origin of the dacite. Instead, we focus on shallow (~3–6 kbars) melting studies.

A considerable number of workers have now studied the dehydration melting reactions of various types of graywackes (e.g., Vielzeuf and Montel 1994; Patiño Douce and Beard 1996; Stevens et al. 1997). Clemens (2006) provides a recent summary of this work; in general, at granulite facies conditions, metagraywacke compositions melt incongruently via the following example reaction: $Bt \pm Hbl + Pl + Qtz = Opx \pm Cpx \pm Grt/Crd/Spl \pm Kfs + M$. Quartz and plagioclase are often still present at the end of these experiments, while K-feldspars are thought to form, but K is generally accommodated in plagioclase as a high Or content. This reaction is highly pressure dependent, and whether garnet, cordierite, or Al-spinel form is a complex manifestation of bulk composition and intensive parameters (Patiño Douce and Beard 1996). The melt productivity of this reaction is largely dictated by the amount of biotite available for dehydration (although the amounts of quartz and plagioclase can have a large influence as well; see Gardien et al. 1995). While the presence of muscovite can produce large amounts of melting at relatively low temperatures, these melts will tend to be far too peraluminous producing leucogranitic melts rather than a weakly metaluminous melt (Patiño Douce 1999), such as the Omega dacite. Similarly, water-present melting experiments by Beard and Lofgren (1991) produced strongly peraluminous melts, causing these authors to infer that melting such compositions is unlikely to be responsible for producing most arc-related silicic rocks.

Numerous experiments have also examined the dehydration melting of various mafic to felsic amphibolites, gneisses, and meta-igneous compositions (e.g., Beard and Lofgren 1991; Patiño Douce and Beard 1995; Koester et al. 2002). Combining a few example reactions summarized in Clemens (2006), the breakdown of hydrous minerals is now extended to hornblende, for general alumina-poor quartzofeldspathic rocks: $Bt \pm Hbl + Pl + Qtz = Cpx \pm Opx \pm Hbl \pm Grt \pm Kfs + M$ and for basaltic to andesitic amphibolites: $Hbl \pm Pl = Opx + Cpx \pm Pl \pm Grt \pm Q + M$. While quartzo-feldspathic rocks still require dehydration of biotite, more mafic compositions often do not contain micas, and so hornblende substitutes. Just as biotite breaks down at a higher temperature than muscovite, hornblende breaks down at still higher temperatures than biotite. Indeed, often temperatures in excess of 900–1,000 °C are required, which is somewhat hotter than the Omega dacite, and much hotter than other silicic magmas erupted throughout the TVZ. Brown et al. (1998) report the presence of both biotite and hornblende variably occurring through the Whakamaru ignimbrites, whose plutonic root is the proposed source of about 40 % of the Omega zircon population. However, since neither hornblende nor biotite is preserved in the Omega dacite, these minerals (along with any quartz) would have to be completely consumed during melting. Moreover, as previously discussed in the context of garnet, Omega REE data do not provide evidence for significant residual amphibole in the Omega source. Finally, if the hygrometer's prediction that the Omega melt contained ≤4–5 wt% H_2O is true, an additional source of water other than that produced during dehydration melting of hydrous phases alone would be necessary.

Due to the lack of preservation of any hydrous phases or quartz, dehydration melting via biotite and/or hornblende breakdown would have run to completion in the Omega magma. Such extensive melting requires an adequate heat source. As shown in the previous section, intrusion of basalt results in far more efficient crustal melting than intrusion of more intermediate compositions, such as dacite. Yet, even in the basaltic intrusion models producing the highest amounts of mobile magma in 10 years (ambient crustal temperatures of 600 °C and radii of 500 and 250 m, Fig. 11), at least 80 % of the total mobile magma must be residual to the more mafic parent.

While many eruptive units do show obvious evidence for interactions with a mobile mafic magma (i.e., the Matahina, Deering 2009; Deering et al. 2011b; the Oruanui, Wilson et al. 2006), the Omega dacite, mineralogically and chemically, does not. The Fe–Ti oxides, which equilibrate rapidly (days to weeks), do not record temperatures significantly different from the pyroxenes (Fig. 6), thus also providing no evidence for rapid and extensive reheating during a 1–10 year remobilization period. While the presence of glomerocrysts may be interpreted as incomplete disaggregation of country rock, the Omega's unimodal mineral chemistry and plagioclase textures/zoning patterns, which are diverse, but equally distributed between glomerocrysts *and* phenocrysts (Fig. 5), require that glomerocrysts share a genetic relationship with individual phenocrysts. Hence, a rapid and extensive crustal melting episode facilitated by a cryptic heat source that results in a fortuitously self-consistent and homogenous crystal population and melt chemistry appears as an unlikely scenario.

The 'down-temperature' crystallization model

In the previous sections, we provided evidence that refutes a model in which the majority of the crystallinity in the Omega dacite was formed from a partially melted, mixed restitic source. Here, we evaluate the opposite end-member: that the majority of the crystallinity was formed via down-temperature crystallization from a more dacitic parent magma, which is accompanied by minor assimilation. As mentioned previously and shown in Fig. 3, plagioclase compositions are largely constrained to $An_{50–60}$, albeit with a trailing of analyses up to higher An contents. Upon close inspection (Fig. 5b, in particular, the inset, and Fig. 5e), it is clear that these high An analyses were not from individual high An grains. Instead, they are grains that have a mixture of 'normal' $An_{\sim 55}$ portions as well as high An diffuse zones. As seen in Fig. 5e, the high An zones frequently occur in the center of the crystal or glomerocryst, precluding late resorption and regrowth via mingling with a mafic magma (which is also not supported in glass or melt inclusion compositions) as a viable interpretation for their formation. Instead, these high An analyses may represent parts of crystals that had formed in a more mafic parent magma or underlying, lower-crustal mush, and were later partially resorbed and overgrown by more evolved, but normally zoned rims. Alternatively, they could represent annealed crystals of different populations from upper-crustal lithologies; however, this interpretation implies only a small volume of crystals from the high An source and a notable paucity of low An sources. Finally, the pervasive normal zoning patterns characterizing the plagioclase population are consistent with a common, down-temperature crystallization episode with uniform changes in intensive parameters and composition throughout the magma body.

Texturally, crystals are largely euhedral to subhedral and have variable amounts of melt inclusions. Some plagioclase grains show a prominent resorption feature (Fig. 5d, e), and occasional plagioclase grains show corroded cores (but overgrown by normally zoned rims). However, large embayments, reaction rims, or pervasively corroded crystals are not frequently observed, as one would expect from interactions with mafic magmas. This provides further support for crystals dominantly representing true *phenocrysts*. In this context, the presence of glomerocrysts can be interpreted in two ways:

1. Cogenetic debris, either from reincorporated, partially solidified wall/roof magma or incorporated pieces of the underlying mush (as opposed to composite non-melted pieces of assimilated country rock; Hogan 1993; Seaman 2000). This is supported by the similarities in chemical composition and texture between minerals in glomerocrysts and those occurring as single phenocrysts.
2. Fragments of country rocks, which reacted peritectically with the melt to form the observed melt assemblage (e.g., reactive bulk assimilation, see Beard et al. 2005; Erdmann et al. 2012). The textures observed by Erdmann et al. (2012) featuring xenocrysts, which are partially replaced and overgrown by peritectic phases (their Figures 12 and 14), are similar qualitatively to those observed in Fig. 5b, e.

It is important to note even in the latter of these cases, however, that the volume of glomerocrysts ($\sim$50 vol% of the crystal cargo) most likely does not directly correlate with the volume of assimilated material (Wolff et al. 1999), which would imply a large quantity of cold stoping fragments whose cooling effect would inevitably lead to further growth of true phenocrysts. Hence, we infer that the majority of the crystals grew in the Omega melt dominantly as phenocrysts, with glomerocrysts mostly derived from disaggregating a high crystallinity rind of the magma

reservoir, with a subordinate number forming as nucleating crystals surrounding assimilated and reacted country rock. We conclude, from petrographic and mineralogical observations, that the Omega dacite is dominated by a single population of crystallizing material, with crystal rims that are in apparent equilibrium with the surrounding homogenous glass. An alternative in which the majority of the crystallinity is simply preserved following large-scale melting requires remarkable chemical homogeneity and euhedral faces on large phenocrysts in the crystal cargo of potential source lithologies, which seems unlikely. Furthermore, we note that zircons, which are not in equilibrium, *are* preserved (although rare), while quartz, K-feldspar, micas, and hornblende (which should be ubiquitous in both the Whakamaru source and the greywackes) are not. Either these phases melted or reacted to completion, while zircons somehow did not, or, more likely, they do exist but are simply hard to detect due also to their small quantity, reflecting the limited role of assimilation in upper-crustal magma evolution.

Thermal models that were aimed at examining this 'down-temperature' assimilation model considered the intrusion of dacitic magma, produced in the mid-to-lower crust (Deering et al. 2011b), instead of basalt. Our results indicate that dacitic intrusions are inefficient as sources of heat for producing significant quantities of wholesale crustal melt. When considering the volumes of mobile magma that can be formed and/or preserved, stock-like intrusion geometries insulate a hot core of magma from heat loss to the crust, maximizing magma longevity. Preservation of dacitic mobile magma in the 1–10 year timescale is possible (Fig. 11), although this magma contains very little crustal material, with at least a 4:1 ratio of intrusive over crustal sources. From this, we conclude that thermal models directed at a down-temperature crystallization path via intrusion of dacite necessarily imply a subordinate role of crustal anatexis in the formation of the Omega magma, which is consistent with the scarcity of xenocrysts in the magma and the other geochemical and petrological interpretations outlined above.

Conclusion

This work examines the bulk crystal cargo of the 20 ka, 0.1 km^3 Omega dacite, reporting detailed mineral chemistry and determining appropriate ranges for intensive parameters. Using petrographic observations, mineral chemistry, and thermodynamic modeling (with the MELTS software), we argue that the overwhelming majority of the crystal population (plagioclase, two pyroxenes, and Fe–Ti oxides) is in petrological equilibrium with the observed melt at eruption, and the dominantly unimodal mineral compositions with normal zoning patterns are consistent with a down-temperature evolution model. We utilized thermal models to provide limits on the extent of crustal melting involved in formation of the Omega dacite, assuming two end-member models: (1) wholesale crustal melting as the dominant mass source, with a 'hot plate' basaltic heat source and (2) down-temperature evolution of a mid-to-lower crustal dacite as the main source of the Omega magma, which only allows minor bulk assimilation of adjacent country rock.

Our observations, incorporating petrography, mineralogy, and thermal modeling, bring further support to an interpretation in which the Omega dacite is generated in a mid-to-lower crustal mush environment via fractional crystallization, with minor assimilation occurring along the way (including minor amounts in the upper-crust). Rather than supporting upper-crustal wholesale melting, this work supports and further characterizes the processes of secondary assimilation ultimately responsible for the liberation of the xenocrystic zircons observed by Charlier et al. (2010). Our interpretation is consistent with many models of magma evolution in arc settings (e.g., Gill 1981; Bacon and Druitt 1988; Hildreth and Moorbath 1988; Annen et al. 2006; Bacon et al. 2007; Jagoutz et al. 2009) including Deering et al. (2011a) for the TVZ, which stress the polybaric, open-system nature of a differentiating crustal column, with intermediate magmas generated in the deeper part of the crust, and the most silicic magmas (rhyolite) in upper-crustal storage zones.

While rare and volumetrically small, magmas with intermediate compositions (such as the Omega dacite), erupting in areas dominated by highly evolved rhyolites, represent an expected shift in the volcanic expression of the large-scale, mushy magma reservoir model (for example, the Kos–Nisyros system see Bachmann et al. 2012; the Long Valley system see Hildreth 2004; the Okataina Volcanic Centre see Shane et al. 2005; and the overall recent TVZ trends see Smith et al. 2005). Such intermediate magmas commonly erupt shortly after large, caldera-forming events. This is an anticipated shift following supervolcanic eruptions, such as the Oruanui event, due to significant, rapid, syn-eruptive, decompression-induced crystallization, which is likely to occur in the non-erupted, gas-saturated, upper-crustal mush (e.g., Bachmann et al. 2012). Hence, the 'rhyolite factory' that allowed the construction of a large, silicic magma body becomes choked with crystals and no longer available for either eruption or efficient melt extraction, until new recharging magma rebuilds the system. We hypothesize that the Omega dacite represents one such mid-to-lower crustal recharge that (1) has been able to erupt, passing through the largely crystalline (and hence brittle) post-Oruanui mush zone, and (2) is a part of a continual sequence of intruding magma which

have collectively been rebuilding an upper-crustal mush, ultimately allowing a return to rhyolite production and volcanism in the TVZ.

Acknowledgments J. S. Beard and an anonymous reviewer are gratefully acknowledged for their thoughtful suggestions and comments that improved this manuscript. This work has been partially supported by the U.S. National Science Foundation (DGE-0718124 to Gelman and 1249821 to Deering) and the Swiss National Science foundation (project 200021_146268 to Bachmann). Darren Gravely is thanked for his help during sampling.

References

Annen C, Blundy JD, Sparks RSJ (2006) The genesis of intermediate and silicic magmas in deep crustal hot zones. J Petrol 47(3):505–539. doi:10.1093/petrology/egi084

Babeyko AY, Sobolev SV, Trumbull RB, Oncken O, Lavier LL (2002) Numerical models of crustal scale convection and partial melting beneath the Altiplano-Puna plateau. Earth Planet Sci Lett 199:373–388

Bachmann O, Schoene B, Schnyder C, Spikings R (2010) The 40Ar/39Ar and U/Pb dating of young rhyolites in the Kos–Nisyros volcanic complex, Eastern Aegean Arc, Greece: age discordance due to excess 40Ar in biotite. Geochem Geophys Geosyst 11:Q0AA08. doi:10.1029/2010GC003073

Bachmann O, Deering CD, Ruprecht JS, Huber C, Skopelitis A, Schnyder C (2012) Evolution of silicic magmas in the Kos–Nisyros volcanic center, Greece: a petrological cycle associated with caldera collapse. Contrib Miner Petrol 163(1):151–166. doi:10.1007/s00410-011-0663-y

Bacon CR, Druitt TH (1988) Compositional evolution of the zoned calcalkaline magma chamber of Mount Mazama, Crater Lake, Oregon. Contrib Miner Petrol 98:224–256

Bacon CR, Hirschmann MM (1988) Mg/Mn partitioning as a test for equilibrium between coexisting Fe–Ti oxides. Am Miner 73:57–61

Bacon CR, Sisson TW, Mazdab FK (2007) Young cumulate complex beneath Veniaminof caldera, Aleutian arc, dated by zircon in erupted plutonic blocks. Geology 35(6):491. doi:10.1130/G23446A.1

Beard JS, Lofgren GE (1991) Dehydration melting and water-saturated melting of basaltic and andesitic greenstones and amphiboles at 1, 3, and 6.9 kb. J Petrol 32(2):365

Beard JS, Ragland PC, Crawford ML (2005) Reactive bulk assimilation: a model for crust-mantle mixing in silicic magmas. Geology 33(8):681–684

Bergantz GW (1989) Underplating and partial melting: implications for melt generation and extraction. Science 245:1093–1095

Bindeman IN, Valley JW (2001) Low delta-18O rhyolites from yellowstone: magmatic evolution based on analyses of zircons and individual phenocrysts. J Petrol 42(8):1491–1517

Blattner P, Rui-Zhong H, Graham IJ, Houston-Eleftheriadis C (1996) Temperatures and isotopic evolutions of silicic magmas, Taupo Volcanic Zone and Coromandel, New Zealand. NZ J Geol Geophys 39:353–362

Bowen NL (1928) The evolution of igneous rocks. Dover, New York

Brown SJA, Wilson CJN, Cole JW, Wooden J (1998) The Whakamaru group ignimbrites, Taupo Volcanic Zone, New Zealand: evidence for reverse tapping of a zoned silicic magmatic system. J Volcanol Geoth Res 84:1–37

Bunsen R (1851) Ueber die prozesse der vulkanishen Gesteinsbildungen Islands. Ann Phys 83:197–272. doi:10.1002/andp.18511590602

Charlier BLA, Wilson CJN, Lowenstern JB, Blake S, VanCalsteren PW, Davidson JP (2005) Magma generation at a large, hyperactive silicic volcano (Taupo, New Zealand) revealed by U–Th and U–Pb systematics in zircons. J Petrol 46(1):3–32

Charlier BLA, Bachmann O, Davidson JP, Dungan MA, Morgan DJ (2007) The upper crustal evolution of a large silicic magma body: evidence from crystal-scale Rb Sr isotopic heterogeneities in the fish canyon magmatic system, Colorado. JPetrol 48(10):1875–1894. doi:10.1093/petrology/egm043

Charlier BLA, Wilson CJN, Davidson JP (2008) Rapid open-system assembly of a large silicic magma body: time-resolved evidence from cored plagioclase crystals in the Oruanui eruption deposits, New Zealand. Contrib Miner Petrol 156(6):799–813. doi:10.1007/s00410-008-0316-y

Charlier BLA, Wilson CJN, Mortimer N (2010) Evidence from zircon U–Pb age spectra for crustal structure and felsic magma genesis at Taupo volcano, New Zealand. Geology 38:915–918

Chesner CA (1998) Petrogenesis of the Toba Tuffs, Sumatra, Indonesia. J Petrol 39(3):397–438

Clemens JD (2006) Melting of the continental crust: fluid regimes, melting reactions and source-rock fertility. In: Brown M, Rushmer T (eds) Evolution and differentiation of the continental crust. Cambridge University Press, Cambridge, pp 397–331

Conrad WK, Nicholls IA, Wall VJ (1988) Water-saturated and -undersaturated melting of metaluminous and peraluminous crustal compositions at 10 kb: evidence for the origin of silicic magmas in the Taupo Volcanic Zone, New Zealand, and other occurrences. J Petrol 29(4):765–803

Costa F, Scaillet B, Pichavant M (2004) Petrological and experimental constraints on the pre-eruptive conditions of Holocene dacite from Volcan San Pedro (36S, Chilean Andes) and the importance of sulfur in silicic subduction-related magmas. J Petrol 45(4):855–881

Daly RA (1914) Igneous rocks and their origin. McGraw-Hill, New York

Darby DJ, Hodgkinson KM, Blick GH (2000) Geodetic measurement of deformation in the Taupo Volcanic Zone, New Zealand: the north Taupo network revisited. NZ J Geol Geophys 43(2):157–170. doi:10.1080/00288306.2000.9514878

Davidson JP, Morgan DJ, Charlier BLA, Harlou R, Hora JM (2007) Microsampling and isotopic analysis of igneous rocks: implications for the study of magmatic systems. Annu Rev Earth Planet Sci 35:273–311

Deering CD (2009) Cannibalization of an amphibole-rich andesitic progenitor induced by caldera-collapse during the Matahina eruption: evidence from amphibole compositions. Am Miner 94(8–9):1162–1174. doi:10.2138/am.2009.3135

Deering CD, Cole JW, Vogel TA (2008) A rhyolite compositional continuum governed by lower crustal source conditions in the Taupo Volcanic Zone, New Zealand. J Petrol 49(12):2245–2276. doi:10.1093/petrology/egn067

Deering CD, Bachmann O, Dufek J, Gravley DM (2011a) Rift-related transition from andesite to rhyolite volcanism in the Taupo Volcanic Zone (New Zealand) controlled by crystal-melt dynamics in mush zones with variable mineral assemblages. J Petrol 52(11):2243–2263. doi:10.1093/petrology/egr046

Deering CD, Cole JW, Vogel TA (2011b) Extraction of crystal-poor rhyolite from a hornblende-bearing intermediate mush: a case study of the caldera-forming Matahina eruption, Okataina volcanic complex. Contrib Miner Petrol 161(1):129–151. doi:10.1007/s00410-010-0524-0

Drummond MS, Defant MJ (1990) A model for trondhjemite–tonalite–dacite genesis and crustal growth via slab melting:

Archean to modern comparisons. J Geophys Res 95(B13):21503–21521
Dufek J, Bachmann O (2010) Quantum magmatism: magmatic compositional gaps generated by melt-crystal dynamics. Geology 38(8):687–690. doi:10.1130/G30831.1
Dufek J, Bergantz GW (2005) Lower crustal magma genesis and preservation: a stochastic framework for the evaluation of basalt-crust interaction. J Petrol 46(11):2167–2195
Dungan MA, Davidson J (2004) Partial assimilative recycling of the mafic plutonic roots of arc volcanoes: an example from the Chilean Andes. Geology 32(9):773. doi:10.1130/G20735.1
Eggler DH (1972) Amphibole stability in H_2O-undersaturated calc-alkaline melts. Earth Planet Sci Lett 15:28–34
Erdmann S, Scaillet B, Kellett DA (2012) Textures of peritectic crystals as guides to reactive minerals in magmatic systems: new insights from melting experiments. J Petrol 53(11):2231–2258. doi:10.1093/petrology/egs048
Ewart A, Stipp JJ (1968) Petrogenesis of the volcanic rocks of the Central North Island, New Zealand, as indicated by a study of Sr87/Sr86 ratios, and Sr, Rb, K, U and Th abundances. Geochim Cosmochim Acta 32:699–736
Francis PW, Thorpe RS, Moorbath S, Kretzschmar GA, Hammill M (1980) Strontium isotope evidence for crustal contamination of calc-alkaline volcanic rocks from Cerro Galan, Northwest Argentina. Earth Planet Sci Lett 48:257–267
Gamble JA, Smith IEM, McCulloch MT, Graham IJ, Kokelaar BP (1993) The geochemistry and petrogenesis of basalts from the Taupo Volcanic Zone and Kermadec Island Arc, S.W. Pacific. J Volcanol Geoth Res 54:265–290
Gardien V, Thompson AB, Grujic D, Ulmer P (1995) Experimental melting of biotite + plagioclase + quartz ± muscovite assemblages and implications for crustal melting. J Geophys Res 100(B8):15581–15591
Geist D, Naumann T, Larson P (1998) Evolution of Galapagos magmas: mantle and crustal fractionation without assimilation. J Petrol 39(5):953–971
Geschwind C-H, Rutherford MJ (1992) Cummingtonite and the evolution of the Mount St. Helens (Washington) magma system: an experimental study. Geology 20:1011–1014
Ghiorso MS, Evans BW (2008) Thermodynamics of Rhombohedral oxide solid solutions and a revision of the FE–TI two-oxide geothermometer and oxygen-barometer. Am J Sci 308(9):957–1039. doi:10.2475/09.2008.01
Ghiorso MS, Sack RO (1995) Chemical mass transfer in magmatic processes IV. A revised and internally consistent thermodynamic model for the interpolation and extrapolation of liquid–solid equilibria in magmatic systems at elevated temperatures and pressures. Contrib Miner Petrol 119:197–212
Gill JB (1981) Orogenic andesites and plate tectonics. Springer, New York
Graham IJ, Gulson BL, Hedenquist JW, Mizon K (1992) Petrogenesis of Late Cenozoic volcanic rocks from the Taupo Volcanic Zone, New Zealand, in the light of new lead isotope data. Geochim Cosmochim Acta 56:2797–2819
Graham IJ, Cole JW, Briggs RM, Gamble JA, Smith IEM (1995) Petrology and petrogenesis of volcanic rocks from the Taupo Volcanic Zone: a review. J Volcanol Geoth Res 68:59–87
Gualda GAR, Ghiorso MS, Lemons RV, Carley TL (2012) Rhyolite-MELTS: a modified calibration of MELTS optimized for silica-rich, fluid-bearing magmatic systems. J Petrol 53(5):875–890. doi:10.1093/petrology/egr080
Gutierrez F, Parada MA (2010) Numerical modeling of time-dependent fluid dynamics and differentiation of a shallow basaltic magma chamber. J Petrol 51(3):731–762. doi:10.1093/petrology/egp101
Haase KM, Stroncik N, Garbe-Schnberg D, Stoffers P (2006) Formation of island arc dacite magmas by extreme crystal fractionation: an example from Brothers Seamount, Kermadec island arc (SW Pacific). J Volcanol Geoth Res 152(3–4):316–330
Halliday AN, Davidson JP, Hildreth W, Holden P (1991) Modelling the petrogenesis of high Rb/Sr silicic magmas. Chem Geol 92:107–114
Harrison AJ, White RS (2004) Crustal structure of the Taupo Volcanic Zone, New Zealand: stretching and igneous intrusion. Geophys Res Lett 31:L13615. doi:10.1029/2004GL019885
Harrison A, White RS (2006) Lithospheric structure of an active backarc basin: the Taupo Volcanic Zone, New Zealand. Geophys J Int 167(2):968–990. doi:10.1111/j.1365-246X.2006.03166.x
Hildreth W (2004) Volcanological perspectives on long valley, Mammoth Mountain, and Mono Craters: several contiguous but discrete systems. J Volcanol Geoth Res 136:169–198. doi:10.1016/j.jvolgeores.2004.05.019
Hildreth W, Moorbath S (1988) Crustal contributions to arc magmatism in the Andes of Central Chile. Contrib Miner Petrol 98:455–489
Hogan JP (1993) Monomineralic glomerocrysts: textural evidence for mineral resorption during crystallization of igneous rocks. J Geol 101(4):531–540
Huber C, Bachmann O, Manga M (2010) Two competing effects of volatiles on heat transfer in crystal-rich magmas: thermal insulation vs defrosting. J Petrol 51(4):847–867. doi:10.1093/petrology/egq003
Huppert HE, Sparks RSJ (1988) The generation of granitic magmas by intrusion of basalt into continental crust. J Petrol 29(3):599–624
Jagoutz OE, Burg J-P, Hussain S, Dawood H, Pettke T, Iizuka T, Maruyama S (2009) Construction of the granitoid crust of an island arc part I: geochronological and geochemical constraints from the plutonic Kohistan (NW Pakistan). Contrib Miner Petrol 158(6):739–755. doi:10.1007/s00410-009-0408-3
Koester E, Pawley AR, Fernandes LAD, Porcher CC, Soliani E (2002) Experimental melting of cordierite gneiss and the petrogenesis of syntranscurrent peraluminous granites in southern Brazil. J Petrol 43(8):1595–1616
Lange RA, Frey HM, Hector J (2009) A thermodynamic model for the plagioclase-liquid hygrometer/thermometer. Am Mineral 94:494–506
Lanphere MA, Baadsgaard H (2001) Precise K–Ar, 40Ar/39Ar, Rb–Sr, and U/Pb mineral ages from the 27.5 Fish Canyon Tuff reference standard. Chem Geol 175:653–671
Marsh BD (1981) On the crystallinity, probability of occurrence, and rheology of lava and magma. Contrib Miner Petrol 78:85–98
Martin H (1999) Adakitic magmas: modern analogues of Archean granitoids. Lithos 46:411–429
McCormack KD, Gee MAM, Mcnaughton NJ, Smith R, Fletcher IR (2009) U–Pb dating of magmatic and xenocryst zircons from Mangakino ignimbrites and their correlation with detrital zircons from the Torlesse metasediments, Taupo Volcanic Zone, New Zealand. J Volcanol Geoth Res 183(1–2):97–111. doi:10.1016/j.jvolgeores.2009.03.005
McCulloch MT, Kyser TK, Woodhead JD, Kinsley L (1994) Pb–Sr–Nd–O isotopic constraints on the origin of rhyolites from the Taupo Volcanic Zone of New Zealand: evidence for assimilation followed by fractionation from basalt. Contrib Miner Petrol 115:303–312
McCurry M, Rodgers DW (2009) Mass transfer along the Yellowstone hot spot track I: Petrologic constraints on the volume of mantle-derived magma. J Volcanol Geotherm Res, 1–13. doi:10.1016/j.jvolgeores.2009.04.001
Muntener O, Kelemen PB, Grove TL (2001) The role of H2O during crystallization of primitive arc magmas under uppermost mantle

conditions and genesis of igneous pyroxenites: an experimental study. Contrib Miner Petrol 141:643–658
New Zealand Geological Survey (1972) North Island. Geological map of New Zealand 1: 1,000,000, 1st edn. Department of Scientific and Industrial Research, Wellington, New Zealand
Patiño Douce AE (1999) What do experiments tell us about the relative contributions of crust and mantle to the origin of granitic magmas? Geological Society, London, Special Publications Understanding Granites: Integrating New and Classical Techniques, pp 55–75
Patiño Douce AE, Beard JS (1995) Dehydration-melting of biotite gneiss and quartz amphibolite from 3 to 15 kbar. J Petrol 36(3):707–738
Patiño Douce AE, Beard JS (1996) Effects of P, f(O2) and Mg/Fe ratio on dehydration melting of model metagreywackes. J Petrol 37(5):999–1024
Petford N, Gallagher K (2001) Partial melting of mafic (amphibolitic) lower crust by periodic influx of basaltic magma. Earth Planet Sci Lett 193:483–499
Petford N, Cruden AR, McCaffrey KJW, Vigneresse J-L (2000) Granite magma formation, transport and emplacement in the Earth's crust. Nature 408:669–673
Pichavant M, Costa F, Burgisser A, Scaillet B, Martel C, Poussineau S (2007) Equilibrium scales in silicic to intermediate magmas–Implications for experimental studies. J Petrol 48(10):1955–1972
Pickard AL, Adams CJ, Barley ME (2000) Australian provenance for upper Permian to Cretaceous rocks forming accretionary complexes on the New Zealand sector of the Gondwanaland margin. Aust J Earth Sci 47:987–1007
Price RC, Gamble JA, Smith IEM, Stewart RB, Eggins S, Wright IC (2005) An integrated model for the temporal evolution of andesites and rhyolites and crustal development in New Zealand's North Island. J Volcanol Geoth Res 140:1–24. doi:10.1016/j.jvolgeores.2004.07.013
Putirka KD (2008) Thermometers and barometers for volcanic systems. In: Keith D. Putirka FJT (ed) Minerals, inclusions and volcanic processes, vol 69. Mineralogical Society of America, pp 61–120
Reid F (1983) Origin of the rhyolitic rocks of the Taupo Volcanic Zone, New Zealand. J Volcanol Geoth Res 15:315–338
Riley TR, Leat PT, Pankhurst RJ, Harris C (2001) Origins of large volume rhyolitic volcanism in teh Antarctic Peninsula and Patagonia by crustal melting. J Petrol 42(6):1043–1065
Seaman SJ (2000) Crystal clusters, feldspar glomerocrysts, and magma envelopes in teh Atascosa Lookout lava flow, southern Arizona, USA: recorders of magmatic events. J Petrol 41(5):693–716
Shane P, Smith VC, Nairn IA (2005) High temperature rhyodacites of the 36 ka Hauparu pyroclastic eruption, Okataina Volcanic Centre, New Zealand: change in a silicic magmatic system following caldera collapse. J Volcanol Geoth Res 147:357–376. doi:10.1016/j.jvolgeores.2005.04.015
Simon JI, Reid MR, Young ED (2007) Lead isotopes by LA-MC-ICPMS: tracking the emergence of mantle signatures in an evolving silicic magma system. Geochemica et Cosmochimica Acta 71:2014–2035. doi:10.1016/j.gca.2007.01.023
Sisson TW, Ratajeski K, Hankins WB, Glazner AF (2005) Voluminous granitic magmas from common basaltic sources. Contrib Miner Petrol 148:635–661
Smith VC, Shane P, Nairn IA (2005) Trends in rhyolite geochemistry, mineralogy, and magma storage during the last 50 kyr at Okataina and Taupo volcanic centres, Taupo Volcanic Zone, New Zealand. J Volcanol Geoth Res 148:372–406. doi:10.1016/j.jvolgeores.2005.05.005
Smith IEM, Worthington TJ, Price RC, Stewart RB, Maas R (2006) Petrogenesis of dacite in an oceanic subduction environment: Raoul Island, Kermadec arc. J Volcanol Geoth Res 156(3–4):252–265
Spera FJ (2000) Physical properties of magma. In: Sigurdsson H (ed) Encyclopedia of volcanoes. Academic Press, New York, pp 171–190
Spera FJ, Bohrson WA (2004) Open-system magma chamber evolution: an energy-constrained geochemical model incorporating the effects of concurrent eruption, recharge, variable assimilation and fractional crystallization (EC-E'RA FC). J Petrol 45(12):2459–2480. doi:10.1093/petrology/egh072
Stevens G, Clemens JD, Droop GTR (1997) Melt production during granulite-facies anatexis: experimental data from "primitive" metasedimentary protoliths. Contrib Miner Petrol 128:352–370
Stratford WR, Stern TA (2006) Crust and upper mantle structure of a continental backarc: central North Island, New Zealand. Geophys J Int 166(1):469–484. doi:10.1111/j.1365-246X.2006.02967.x
Sutton AN, Blake S, Wilson CJN (1995) An outline geochemistry of rhyolite eruptives from Taupo volcanic centre, New Zealand. J Volcanol Geoth Res 68:153–175
Sutton AN, Blake S, Wilson CJN, Charlier BLA (2000) Late quaternary evolution of a hyperactive rhyolite magmatic system: Taupo Volcanic centre, New Zealand. J Geol Soc Lond 157:537–552
Taylor HP (1980) The effects of assimilation of country rocks by magmas on 18O/16O and 87Sr/86Sr systematics in igneous rocks. Earth Planet Sci Lett 47:243–254
Thompson AB, Connolly JAD (1995) Melting of the continental crust: some thermal and petrological constraints on anatexis in continental collision zones and other tectonic settings. J Geophys Res 100(B8):15565–15579
Vielzeuf D, Montel JM (1994) Partial melting of metagreywackes. Part I. Fluid-absent experiments and phase relationships. Contrib Mineral Petrol 117(4):375–393
Whittington AG, Hofmeister AM, Nabelek PI (2009) Temperature-dependent thermal diffusivity of the Earth's crust and implications for magmatism. Nature 458(7236):319–321. doi:10.1038/nature07818
Wilson CJN (1993) Stratigraphy, chronology, styles and dynamics of late Quaternary eruptions from taupo volcano, New Zealand. Philos Trans: Phys Sci Eng 343(1668):205–306
Wilson CJN, Houghton BF, McWilliams MO, Lanphere MA, Weaver SD, Briggs RM (1995) Volcanic and structural evolution of Taupo Volcanic Zone: a review. J Volcanol Geoth Res 68:1–28
Wilson CJN, Blake S, Charlier BLA, Sutton AN (2006) The 26.5 ka Oruanui eruption, Taupo volcano, New Zealand: development, characteristics and evacuation of a large rhyolitic magma body. J Petrol 47(1):35–69. doi:10.1093/petrology/egi066
Wolff JA, Ramos FC, Davidson JP (1999) Sr isotope disequilibrium during differentiation of the Bandelier Tuff: constraints on the crystallization or a large rhyolitic magma chamber. Geology 27:495–498